







**RESEARCH ARTICLE**

# Novel luminescent Schiff's base derivative with an azo moiety for ultrasensitive and sensitive chemosensor of Fe<sup>3+</sup> ions

Krisfian Tata Aneka Priyanga<sup>1,2</sup>  | Yehezkiel Steven Kurniawan<sup>1</sup>  |  
 Leny Yulianti<sup>1,3</sup>  | Bambang Purwono<sup>2</sup>  | Tutik Dwi Wahyuningsih<sup>2</sup>  |  
 Hendrik O. Lintang<sup>3</sup> 

<sup>1</sup>Ma Chung Research Center for Photosynthetic Pigments, Universitas Ma Chung, Villa Puncak Tidar N-01, Malang, East Java, Indonesia

<sup>2</sup>Department of Chemistry, Faculty of Mathematics and Natural Sciences, Universitas Gadjah Mada, Sekip Utara Bulaksumur, Yogyakarta, Indonesia

<sup>3</sup>Department of Chemistry, Faculty of Science and Technology, Universitas Ma Chung, Villa Puncak Tidar N-01, Malang, East Java, Indonesia

**Correspondence**

Hendrik O. Lintang, Department of Chemistry, Faculty of Science and Technology, Universitas Ma Chung, Villa Puncak Tidar N-01, Malang 65151, East Java, Indonesia.  
 Email: hendrik.lintang@machung.ac.id

**Funding information**

Ministry of Research, Technology, and Higher Education

**Abstract**

Chemosensors with ultrasensing capabilities for detection of metal ions have received particular attention when using luminescent organic compounds. Even though hundreds of chemosensor agents have been reported for Fe<sup>3+</sup> ion sensing, the designs of those molecules have been complicated and time consuming, in addition to having limited application for aquatic samples due to their poor hydrophilicity. Here, we synthesized a novel azo-imine derivative (**L2**) that showed ultrasensitive and selective sensing for Fe<sup>3+</sup> ions. **L2** exhibited ultrasensitive detection of Fe<sup>3+</sup> ions with a turn-off of its emission intensity at 341 nm in H<sub>2</sub>O:MeOH (4:1 v/v) aqueous medium. This quenching phenomenon was in good agreement with its colour change from orange-yellowish to colourless. Its capability was shown due to its very low limit of detection and limit of quantification values of 0.31 and 1.04 μM, respectively. The interference study showed that **L2** is ultrasensitive for the detection of Fe<sup>3+</sup> ions without a significant reduction in its sensing capability even in competitive metal mixtures. Furthermore, direct Fe<sup>3+</sup> quantification of tap and drinking water showed that **L2** gave good recovery percentages. These findings demonstrated that the Schiff's base with an azo fluorophore derivative is a potential chemosensor agent for Fe<sup>3+</sup> ions sensing applications in aqueous media.

**KEYWORDS**

azo-imine, chemosensor, Fe<sup>3+</sup> ions, fluorescence, ultrasensitive

## 1 | INTRODUCTION

Metallurgical industries of iron and steel manufacturing tend to generate large amounts of waste, especially in liquid form containing metallic irons that are released into the aquatic environment.<sup>[1]</sup> Among the other transition metals, iron is a relatively abundant essential ion that has a pivotal role in the area of biological and environmental chemistry.<sup>[2-5]</sup> However, excess intake of iron may cause some health issues such as cancers and dysfunction of several vital organs.<sup>[6]</sup> Fe<sup>3+</sup> ions, as the most stable oxidation state of the iron species, are mainly found in water systems with dissolved oxygen.<sup>[7]</sup> Therefore, the development

of the selective and sensitive detection methods for Fe<sup>3+</sup> ions is critical. In recent years, current research has focused on the design and development of chemosensor agents with high selectivity for detection of Fe<sup>3+</sup> ions.<sup>[8-11]</sup>

Chemosensors with fluorescence properties have received significant attention due to their great advantages such as highly sensitive and selective, as well as the possibility to be used for real-time monitoring.<sup>[12]</sup> Many types of research into chemosensors have been reported based on organic fluorescence receptors for the detection of Fe<sup>3+</sup> ions. However, their synthesis routes are often complicated, and they have had poor limits of detection (LOD) as well as limits of

quantification (LOQ).<sup>[2,8,13–22]</sup> Additionally, several reports have shown low solubility in water, limiting their application for environmental samples. For example, a polyphenyl derivative was synthesized from 2,3,4,5-tetraphenyl-cyclopentenone, which could be used for the fluorescence detection of  $\text{Fe}^{3+}$  ions in ethanol:water (EtOH:H<sub>2</sub>O) at a 10:1 v/v ratio with 4  $\mu\text{M}$  as the LOD value.<sup>[23]</sup> The carbazole-based Schiff's base compound gave better LOD values (3.62  $\mu\text{M}$ ) towards  $\text{Fe}^{3+}$  detection in acetonitrile (CH<sub>3</sub>CN), however other metal ions such as  $\text{Cu}^{2+}$  produced significant interference.<sup>[24]</sup> Additionally, a fluoranthene-based pyridine ligand, synthesized from acenaphthenedione under inert conditions, was used as a fluorescent chemosensor for  $\text{Fe}^{3+}$  ions in EtOH. However, selectivity was inhibited by the presence of other counteranions such as sulfate, which made its use unfavourable.<sup>[25]</sup>

Chemosensor agents based on Schiff's base derivatives with imine or azomethine groups could be simply prepared through condensation reactions between benzaldehyde and amine compounds in a high yield. They also exhibited excellent performance to form complexes by binding to certain metal ions,<sup>[26]</sup> as well as good LOD and LOQ values.<sup>[27,28]</sup> To enhance their capabilities as chemosensors for  $\text{Fe}^{3+}$  ions, many fluorescent chemosensors based on Schiff's bases have focused on their modification with a chromophore group,<sup>[2,8,13–15,18,29,30]</sup> such as rhodamine,<sup>[30]</sup> naphthalimide,<sup>[15]</sup> and coumarin<sup>[14,19]</sup> moieties. Qin *et al.* prepared a fluorescent chemosensor based on a rhodamine–quinoline conjugate in methanol (MeOH) with LOD values as low as 0.83  $\mu\text{M}$  for  $\text{Fe}^{3+}$  detection.<sup>[30]</sup> Other researchers have reported that coupled naphthol containing an azo group ( $-\text{N}=\text{N}$ ) could detect  $\text{Fe}^{3+}$  ions in a 1:1 ratio of CH<sub>3</sub>CN:H<sub>2</sub>O with LOD values as low as 0.937  $\mu\text{M}$ .<sup>[31]</sup>

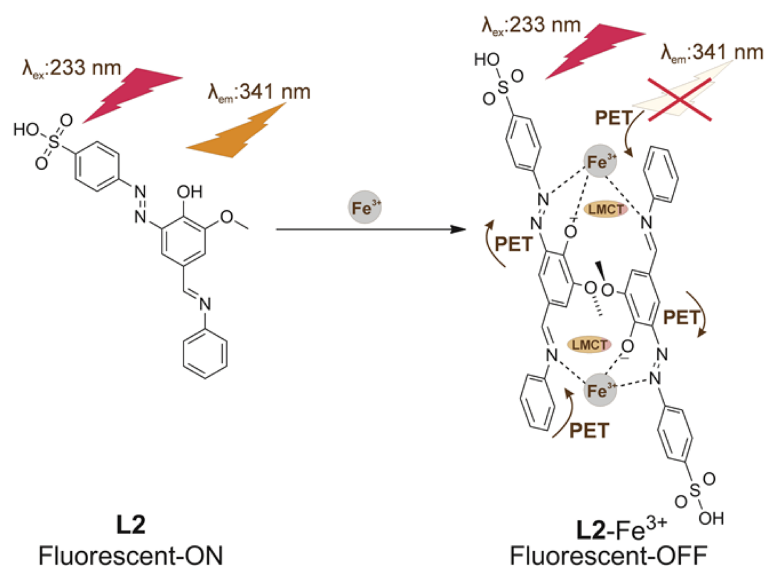
Conversely, azo derivatives have been extensively investigated because of their excellent fluorophore functionalization in dyes and molecular recognition applications. However, a systematic study on fluorescence detection of  $\text{Fe}^{3+}$  ions using modified Schiff's base derivatives consisting of azo fluorophores ( $-\text{N}=\text{N}$ ) has rarely been reported. As an azo moiety is considered as an excellent fluorophore group,<sup>[32]</sup>

a combination of azo-imine moieties on chemosensor agents may serve as an excellent platform for the fluorescence detection and quantification with high selectivity and sensitivity of  $\text{Fe}^{3+}$  ions. Moreover, chemosensors with azo-imine moieties could increase the possibility for real application for environmental samples with the presence of a sulfonic acid functional group.<sup>[33,34]</sup> Therefore, in the present work, we report the first successful synthesis of a Schiff's base azo-imine as a fluorescent chemosensor for  $\text{Fe}^{3+}$  ions in an almost aqueous system. The azo-imine derivative, named as 4-((E)-(2-hydroxy-3-methoxy-5-((E)(phenylimino)methyl)phenyl)diazenyl)benzene sulfonic acid (**L2**) was successfully prepared through simple two-step reactions, diazotization and nucleophilic addition reactions. In particular, the novel chemosensor **L2** showed ultraselective and ultrasensitive properties for detection of  $\text{Fe}^{3+}$  ions through turn-off of its fluorescence properties with quenching of emission intensity at 341 nm (Scheme 1) and with an LOD of 0.31  $\mu\text{M}$  in H<sub>2</sub>O:MeOH (4:1 v/v). Indeed, this chemosensor **L2** could be applied for the quantification of  $\text{Fe}^{3+}$  ions from tap and drinking water as the representations of real samples and with good recovery.

## 2 | EXPERIMENTAL

### 2.1 | Materials

The chemicals used in the present work, such as sulfanilic acid (4-aminobenzene sulfonic acid), anhydrous potassium carbonate (K<sub>2</sub>CO<sub>3</sub>), sodium nitrite (NaNO<sub>2</sub>), vanillin (4-hydroxy-3-methoxybenzaldehyde), aniline, concentrated hydrochloric acid (HCl 37% w/v), sodium hydroxide (NaOH), acetone, MeOH, ethyl acetate (EtOAc), EtOH, metal chloride salts (i.e. KCl, NaCl, ZnCl<sub>2</sub>, MnCl<sub>2</sub>, FeCl<sub>3</sub>, CoCl<sub>2</sub>, NiCl<sub>2</sub>, CuCl<sub>2</sub>, MgCl<sub>2</sub>, CaCl<sub>2</sub>, BaCl<sub>2</sub>, and LaCl<sub>3</sub>) and thin-layer chromatography plate (silica gel 60 F<sub>254</sub>) were purchased from Merck in proanalysis grade and used without further purification.



**SCHEME 1** Schematic sensing mechanism of  $\text{Fe}^{3+}$  ions using Schiff's base azo-imine compound (**L2**) with 1:1 ratio of molecular recognition

## 2.2 | Instrumentation

The instrumentation used in this work were a melting point measurement apparatus (Electrothermal 9100), a Fourier transform infrared (FTIR) spectrometer (Jasco 6800), and a UV-vis spectrophotometer (Jasco V-760), as well as spectrofluorometer (Jasco FP-8500ST). Other instrumentations were a liquid chromatography-high resolution mass spectrometer for liquid chromatography-high resolution mass spectrometry (LC-HRMS) consisting of a high performance liquid chromatography (Thermo Scientific Dionex Ultimate 3000 RSLCnano with microflow meter) and an HRMS system (Thermo Scientific Q Exactive parallel-reaction monitoring with MS2 at 17500 Resolution) with electrospray ionization (ESI), and an  $^1\text{H-NMR}$  and  $^{13}\text{C-NMR}$  spectrometer (Jeol 400 MHz with 5 mm probe) which were used for characterization of molecular structure.

## 2.3 | Synthesis of compound L1

Sulfanilic acid (1.93 g, 11 mmol) and anhydrous  $\text{K}_2\text{CO}_3$  (0.77 g, 5.5 mmol, 0.5 eq.) were dissolved in distilled  $\text{H}_2\text{O}$  (30 ml) and cooled at  $0-5^\circ\text{C}$ . Then, dissolved  $\text{NaNO}_2$  (0.65 g, 11 mmol, 1.0 eq.) and concentrated  $\text{HCl}$  (3.13 ml) in cold distilled  $\text{H}_2\text{O}$  (20 ml) were slowly added (dropwise) to give mixture 1.

Conversely, mixture 2 was prepared by dissolving vanillin (1.70 g, 11 mmol, 1.0 eq.) in  $\text{NaOH}$  10% w/v (6.0 ml) at  $0-5^\circ\text{C}$ . Mixture 1 was added slowly into mixture 2. The new mixture was stirred for 4 h and the formed precipitation was filtered and recrystallized with  $\text{MeOH}$ : $\text{EtOAc}$  in 7:3 v/v to give (E)-4-([5-formyl-2-hydroxy-3-methoxyphenyl] diazenyl)benzene sulfonic acid (**L1**) as a reddish-brown solid at 31% yield (1.13 g). m.p.  $>293^\circ\text{C}$  (decomposed).  $\epsilon_{\text{L1}} = 1.05 \times 10^4 \text{ L mol}^{-1} \text{ cm}^{-1}$ .  $\phi_{\text{L1}} = 0.0019$  in  $\text{H}_2\text{O}:\text{MeOH}$  (4:1 v/v). FTIR (KBr,  $\nu/\text{cm}^{-1}$ ): 3474 ( $-\text{OH}$ ), 3073 (C-H  $\text{sp}^2$ ), 2928 (CH  $\text{sp}^3$ ), 2849 and 2753 (H-C=O), 1692 (C=O), 1601 (C=C aromatic), 1427 (N=N), 1201 (C-O), as well as 1034 and 671 ( $\text{SO}_3\text{H}$ ).  $^1\text{H-NMR}$  ( $\text{DMSO-d}_6$ ,  $\delta/\text{ppm}$ ): 9.88 (s, 1H,  $-\text{CHO}$ ), 9.73 (s, 1H,  $-\text{SO}_3\text{H}$ ), 8.73 (s, 1H, C-OH), 7.99 (d,  $J = 7.16 \text{ Hz}$ , 1H, H aromatic), 7.88 (s, 1H, H aromatic), 7.79 (d,  $J = 7.16 \text{ Hz}$ , 1H, H aromatic), 7.62 (m,  $J = 7.52 \text{ Hz}$ , 1H, H aromatic), 7.50 (s, 1H, H aromatic), 7.37 (m,  $J = 8.28 \text{ Hz}$ , 1H, H aromatic), and 3.17 (s, 3H,  $-\text{OCH}_3$ ).  $^{13}\text{C-NMR}$  ( $\text{DMSO-d}_6$ ,  $\delta/\text{ppm}$ ): 192.11 (C=O), 151.97, 151.43, 150.59, 128.20, 127.56, 127.23, 123.16, 120.82, 116.59, 115.94 and 111.83 (C aromatics), 139.16 (C-OH), and 56.703 ( $-\text{OCH}_3$ ). HRMS: m/z found 335.03445 Da ( $[\text{M-H}]^-$ ) for  $\text{C}_{14}\text{H}_{12}\text{N}_2\text{O}_6\text{S}$  with a theoretical calculation of m/z at 335.03433 Da.

## 2.4 | Synthesis of compound L2

A mixture of **L1** (0.64 g, 2 mmol),  $\text{K}_2\text{CO}_3$  (0.30 g, 2 mmol, 1 eq.) and aniline (2 ml, 2 mmol, 1 eq.) was dissolved in  $\text{EtOH}$  (25 ml) and the mixture was treated under reflux for 8 h. The mixture was evaporated and then neutralized using  $\text{HCl}$  10% v/v. The formed precipitation

was washed with distilled water and recrystallized with acetone to obtain the desired 4-((E)-(2-hydroxy-3-methoxy-5-((E)-(phenylimino) methyl) phenyl)diazanyl)benzene sulfonic acid (**L2**) product as a brownish solid at 71% yield (0.46 g). m.p.  $>293^\circ\text{C}$  (decomposed).  $\epsilon_{\text{L2}} = 2.24 \times 10^4 \text{ L mol}^{-1} \text{ cm}^{-1}$ .  $\phi_{\text{L2}} = 0.0062$  in  $\text{H}_2\text{O}:\text{MeOH}$  (4:1 v/v). FTIR (KBr,  $\text{cm}^{-1}$ ): 3420 ( $-\text{OH}$ ), 3065 (CH  $\text{sp}^2$ ), 2928 and 2854 (CH  $\text{sp}^3$ ), 1661 (C=N), 1586 (C=C), 1428 (N=N), 1305 (C-O), 1031 (C-O), 1010 and 671 ( $\text{SO}_3\text{H}$ ).  $^1\text{H-NMR}$  ( $\text{DMSO-d}_6$ ,  $\delta/\text{ppm}$ ): 9.90 (s, 1H, H-C=N), 9.74 (s, 1H,  $-\text{SO}_3\text{H}$ ), 8.83 (s, 1H, C-OH), 7.99 (d,  $J = 8.24 \text{ Hz}$ , 2H, H aromatic), 7.89 (s, 1H, H aromatic), 7.76 (d,  $J = 8.44 \text{ Hz}$ , 2H, H aromatic), 7.49 (m,  $J = 7.68 \text{ Hz}$ , 1H, H aromatic), 7.47 (s, 1H, H aromatic), 7.45 (m,  $J = 7.76 \text{ Hz}$ , 1H, H aromatic), 7.40 (m,  $J = 6.92 \text{ Hz}$ , 1H, H aromatic), 7.36 (m,  $J = 6.92 \text{ Hz}$ , 1H, H aromatic), 7.30 (d,  $J = 7.36 \text{ Hz}$ , 1H, H aromatic), and 3.17 (s, 3H,  $-\text{OCH}_3$ ).  $^{13}\text{C-NMR}$  ( $\text{DMSO-d}_6$ ,  $\delta/\text{ppm}$ ): 192.10 (C=N), 151.99, 151.40, 150.59, 132.51, 130.01, 130.01, 128.55, 128.26, 127.31, 127.31, 123.70, 123.70, 123.17, 123.17, 121.57, 116.63 and 111.70 (C aromatics), 139.15 (C-OH), and 56.694 ( $-\text{OCH}_3$ ). HRMS: m/z found 410.08163 Da ( $[\text{M-H}]^-$ ) for  $\text{C}_{20}\text{H}_{17}\text{N}_3\text{O}_5\text{S}$  with a theoretical calculation of m/z at 410.08161 Da.

## 2.5 | Sensitivity test for L2 as a chemosensor of $\text{Fe}^{3+}$ ions

The chemosensor **L2** was dissolved in  $\text{H}_2\text{O}:\text{MeOH}$  solvent in a 4:1 v/v ratio at 0.20 mM and called the ligand solution. The ligand solution was arbitrary mixed with  $\text{Fe}^{3+}$  ion solution at 3.0 mM in  $\text{H}_2\text{O}:\text{MeOH}$  (4:1 v/v), giving the final concentration of ligand in the mixture of 0.03 mM. The final concentrations of  $\text{Fe}^{3+}$  ions were prepared in the series of 0, 0.003, 0.006, 0.0075, 0.015, 0.023, 0.024, 0.030, 0.060, 0.075, 0.150, 0.225, 0.240 and 0.30 mM to evaluate sensitivity. To calculate the LOD and LOQ values, Equations 1 and 2 were used as follows:

$$\text{LOD} = 3 \times \text{standard error/slope} \quad (1)$$

$$\text{LOQ} = 10 \times \text{standard error/slope} \quad (2)$$

## 2.6 | Complexation study between chemosensor L2 and $\text{Fe}^{3+}$ ions

The stock solution of chemosensor **L2** at 0.20 mM and the stock solution of  $\text{FeCl}_3$  at 3.00 mM were mixed and diluted at various volume ratios to maintain a total mole fraction of 3.0 ml of **L2** and  $\text{Fe}^{3+}$  mixture at 0.03 mM. The fluorescence spectrum of each mixture was measured using a spectrofluorometer to determine the stoichiometric ratio of the formed complex between **L2** and  $\text{Fe}^{3+}$  ions.

The chemosensor **L2** solution at 0.03 mM was mixed with 3.00 mM of  $\text{Fe}^{3+}$  ion solution. The final concentration of ligand in the mixture was 0.03 mM and the final concentrations of  $\text{Fe}^{3+}$  ions were 0, 0.003, 0.006, 0.0075, 0.015, 0.023, 0.024, 0.030, 0.060, 0.075,

0.150, 0.225, 0.240 and 0.30 mM. The fluorescence spectrum of each mixture was also measured using a spectrofluorometer to construct a Benesi-Hildebrand plot to calculate the association constant between chemosensor **L2** and  $\text{Fe}^{3+}$  ions.

## 2.7 | Selectivity and interference test of chemosensor **L2** for detection of $\text{Fe}^{3+}$ ions

The chemosensor **L2** solution at 0.20 mM was mixed with 15  $\mu\text{l}$  stock solution of metal chloride solutions ( $\text{FeCl}_3$ ,  $\text{NaCl}$ ,  $\text{KCl}$ ,  $\text{MgCl}_2$ ,  $\text{CaCl}_2$ ,  $\text{BaCl}_2$ ,  $\text{MnCl}_2$ ,  $\text{CoCl}_2$ ,  $\text{CuCl}_2$ ,  $\text{NiCl}_2$ ,  $\text{ZnCl}_2$ , and  $\text{LaCl}_3$ ) at 30.0 mM to give a mixture with a total volume of 3 ml in  $\text{H}_2\text{O}:\text{MeOH}$  (4:1 v/v). The fluorescence spectrum of each mixture was measured using a spectrofluorometer to evaluate the selectivity. Furthermore, the interference of the other metal ions on  $\text{Fe}^{3+}$  detection was investigated by mixing  $\text{Fe}^{3+}$  ions at 0.03 mM and other metal ions at 0.15 mM. Interference percentage was calculated using Equation 3 as follows:

$$\text{Interference (\%)} = \frac{\left( \left[ \text{Fe}^{3+} \right]_{\text{observed}} - \left[ \text{Fe}^{3+} \right]_{\text{theoretical}} \right)}{\left[ \text{Fe}^{3+} \right]_{\text{theoretical}}} \times 100\% \quad (3)$$

$\text{Fe}^{3+}$  quantification of the real samples, i.e. tap and drinking water was also carried out similarly as mentioned above.

## 3 | RESULTS AND DISCUSSION

### 3.1 | Synthesis of **L1** and **L2** compounds

Synthesis of **L1** that contains an azo group was carried out through a diazotization reaction between vanillin and sulfanilic acid as precursors. In addition, the **L2** compound was synthesized from a nucleophilic addition (condensation) reaction between **L1** and aniline. First, the diazonium salt of sulfanilic acid was reacted with vanillin under alkaline conditions of  $\text{K}_2\text{CO}_3$  to form **L1**. Next, **L1** was reacted with aniline to produce **L2** (Figure 1). The structure of the products was

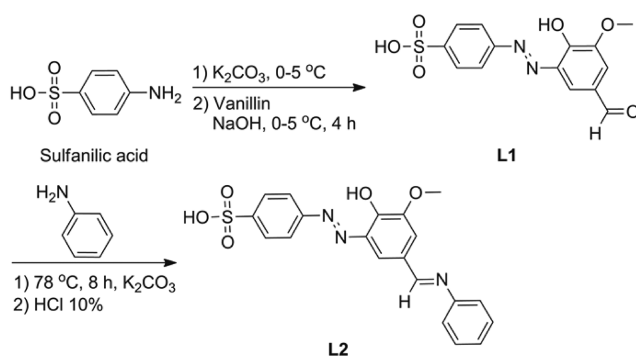


**FIGURE 1** Synthesis scheme of **L1** and **L2** compounds from sulfanilic acid and vanillin

elucidated using FTIR, LC-HRMS, and  $^1\text{H-NMR}$  and  $^{13}\text{C-NMR}$  spectrometry.

The FTIR spectra of **L1** and **L2** are shown in Figure S1. Differing from the FTIR standard of sulfanilic acid as the precursor, the FTIR spectrum of **L1** showed the appearance of a C-H aldehyde functional group at 2849 and 2753  $\text{cm}^{-1}$  and also the existence of C=O aldehyde and N=N azo functional groups at 1692 and 1427  $\text{cm}^{-1}$ . In addition, the C-H aldehyde peaks disappeared on the FTIR spectrum for **L2**, indicating successful synthesis through a condensation reaction. Furthermore, the vibration peak at 1692  $\text{cm}^{-1}$  was shifted to a lower wavenumber (1661  $\text{cm}^{-1}$ ) due to the transformation of C=O aldehyde to C=N Schiff's base. Based on the  $^1\text{H-NMR}$  and  $^{13}\text{C-NMR}$  elucidation (Figures S2-S5), it was confirmed that both **L1** and **L2** compounds had been successfully synthesized. The presence of methoxy and C-H aldehyde protons on **L1**, corresponding to the vanillin moiety, was found at 3.17 and 9.88 ppm as singlet signals. The addition of aromatic protons at 7.30-7.49 ppm corresponded to the aniline moiety of **L2**.  $^{13}\text{C-NMR}$  spectra of **L1** and **L2** confirmed the total number of carbon atoms of each compound, i.e. 14 and 20 carbon atoms, respectively. Further characterization using HRMS spectrometry showed that the  $[\text{M-H}]^-$  of **L1** and **L2** were found at 335.03445 Da and 410.08163 Da, respectively, which was very close to the calculated  $[\text{M-H}]^-$  values for both compounds (335.03433 and 410.08161 Da) with accuracy less than 1 ppm, while the monoisotopic patterns were similar to the predicted ones. From FTIR,  $^1\text{H-NMR}$ ,  $^{13}\text{C-NMR}$ , and HRMS analyses, it was confirmed that the molecular structures of **L1** and **L2** were correctly synthesized and, therefore, had been isolated as pure compounds.

Figure 2 shows the fluorescence spectra of compounds **L1** and **L2** in  $\text{H}_2\text{O}:\text{MeOH}$  (4:1 v/v). Interestingly, the **L1** (black line) gave two excitation peaks (black with dashed line) at 203 and 251 nm corresponding to aromatic and azo ( $-\text{N}=\text{N}$ ) functional groups, while emission peaks were found at 341 and 423 nm (black with solid line).

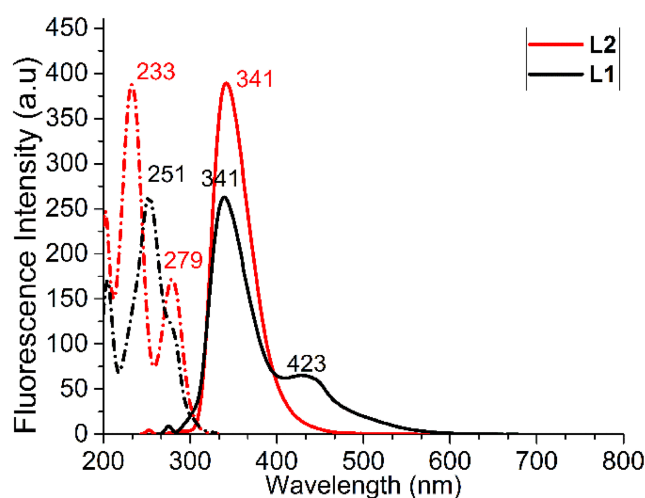


**FIGURE 2** Fluorescence spectrum of **L1** (black line) and **L2** (red line). Dashed and solid lines correspond to excitation and emission spectra, respectively

Conversely, **L2** (red line) showed three excitation peaks at 203, 233, and 279 nm (red with dash line), corresponding to the aromatic, azo ( $-N=N$ ), and imine ( $-C=N$ ) functional groups, respectively. The  $-N=N$  group had a lower excitation wavelength, probably as it was adjacent to a hydroxyl group in the aromatic ring to form a tautomeric azenol<sup>[35]</sup> from the inductive effect. Upon monitoring at 233 and 279 nm (red with solid line), it was found that both excitation wavelengths gave an emission peak at 341 nm, whereas a higher intensity was given using 233 nm. Therefore, further studies have focused on monitoring emission spectral changes with an excitation wavelength at 233 nm. The molar extinction coefficient and fluorescence quantum yield values of **L2** ( $\epsilon_{L2} = 2.24 \times 10^4 \text{ L mol}^{-1} \text{ cm}^{-1}$ ,  $\phi_{L2} = 0.0062$ ) were higher than that of **L1** ( $\epsilon_{L1} = 1.05 \times 10^4 \text{ L mol}^{-1} \text{ cm}^{-1}$ ,  $\phi_{L1} = 0.0019$ ). Fluorescence quantum yield was measured using rhodamine B solution in water as the standard ( $\phi = 0.3100$ ). This means that **L2** had better optical and photoluminescence properties than the **L1** compound. Low fluorescence quantum yield values for Schiff's base derivatives have also been reported in previous studies for the pyrene-Schiff's base and triphenylamine-Schiff's base ( $\phi = 0.0900$ ).<sup>[14,22]</sup>

### 3.2 | Sensing sensitivity of **L2** toward $\text{Fe}^{3+}$ detection and quantification

**L2** was evaluated as a chemosensor agent towards the detection and quantification of  $\text{Fe}^{3+}$  ions. After addition of  $\text{Fe}^{3+}$  ions to **L2** as shown from the fluorescence titration study (Figure 3a,b), it was found that both excitation and emission signals (Figure 3a,b) were gradually quenched by increasing the equivalence of  $\text{Fe}^{3+}$  ions. Moreover, quenching percentage was gradually increased up to almost 100%. Such sensing capability was well supported by decreasing  $\phi_{L2}$  from 0.0062 to 0.000096 (almost 100%). Indeed, these emission and excitation spectral changes were also in good agreement with the colour of the ligand solution from orange-yellowish (before sensing) to colourless upon addition of  $\text{Fe}^{3+}$  ions (Figure 3c), indicating a rapid sensing property of **L2** toward  $\text{Fe}^{3+}$  ions. These colour changes were clearly visualized by the addition of  $\text{Fe}^{3+}$  ions with a concentration of 0.75 eq. From the contact time study with the equilibrium conditions even within a minute, such sensing capability for the rapid detection of  $\text{Fe}^{3+}$  ions (Figure S6) is really important in real-time sample analysis. Of interest, the emission spectral changes showed the same

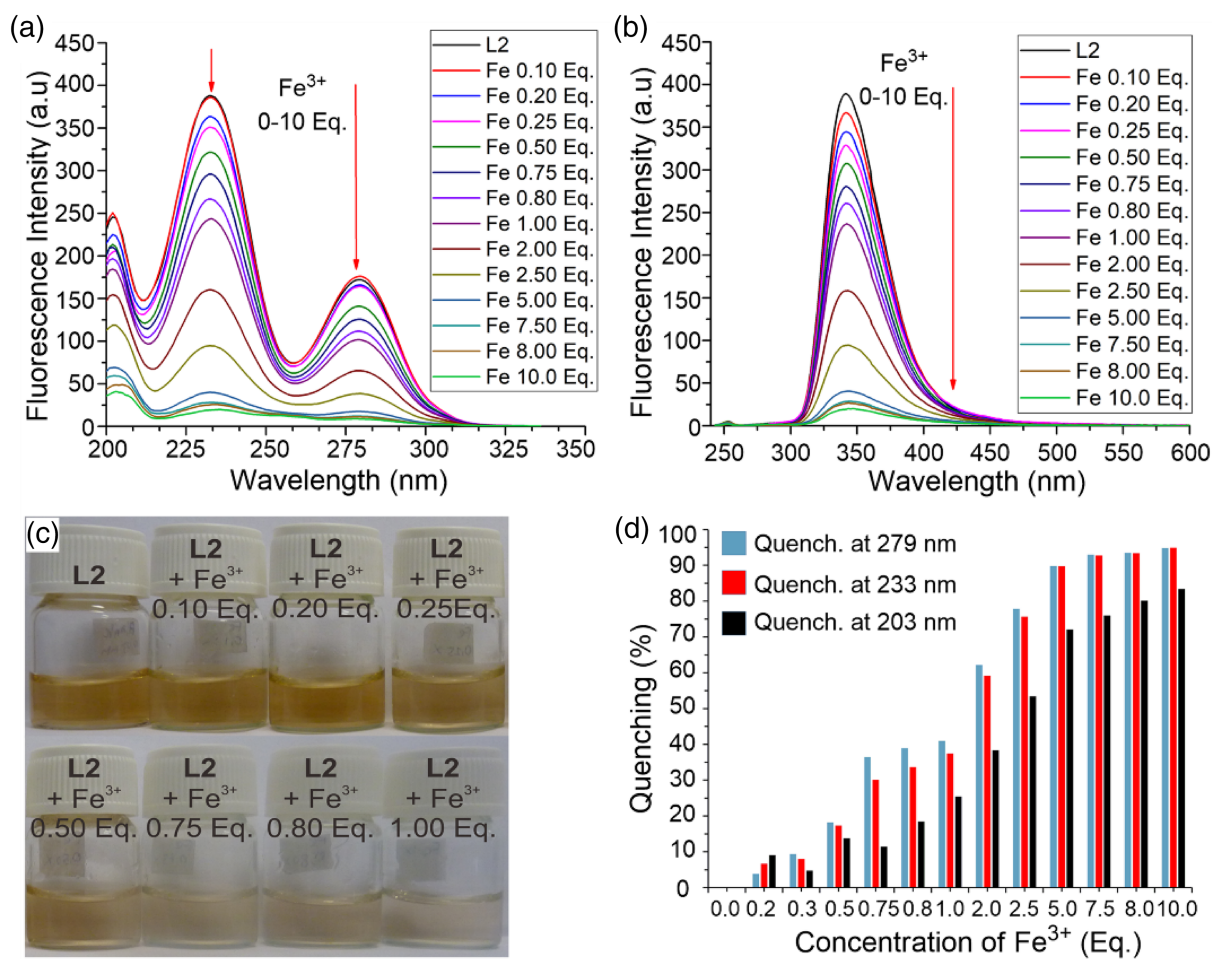


**FIGURE 3** (a) Excitation ( $\lambda_{em} = 341 \text{ nm}$ ); and (b) emission ( $\lambda_{ex} = 233 \text{ nm}$ ) spectral changes of **L2** in  $\text{H}_2\text{O}:\text{MeOH}$  (4:1 v/v) with the addition of  $\text{Fe}^{3+}$  ions (0–10 eq.). (c) Photographs in daylight. (d) Per cent quenching (**L2** = 0.03 mM)

quenching phenomena using different excitation wavelengths (203, 233, and 279 nm), as presented in (Figure 3d).

A Stern–Volmer plot was constructed from the study of fluorescence titration data as the plot of  $I/I_0$  versus  $Fe^{3+}$  ions, where  $I_0$  is

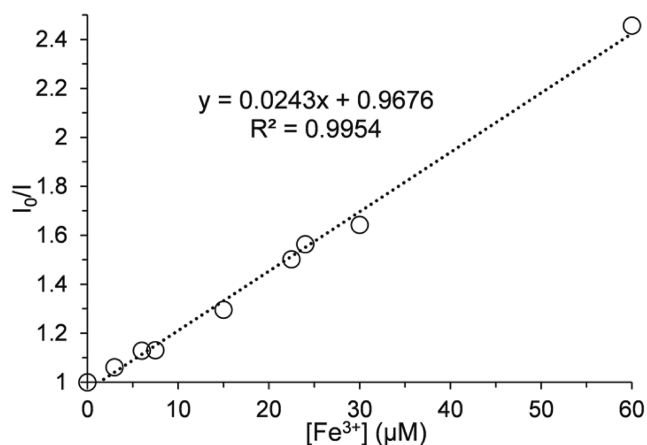


**FIGURE 4** Stern–Volmer plot of **L2** (0.03 mM) with the addition of  $Fe^{3+}$  ions (0–60 μM) in  $H_2O:MeOH$  (4:1 v/v)

initial emission intensity of **L2**, and  $I$  is the emission intensity of **L2** with the addition of  $Fe^{3+}$  ions at various concentrations, with 341 nm as the emission signal. From the Stern–Volmer plot (Figure 4), the LOD and LOQ values were found to be 0.31 and 1.04 μM with a linear dynamic range between 1.0 to 60 μM, which indicated ultrasensitive detection. Moreover, **L2** in fluorescence titration yielded 0–2.5% of % relative standard deviation (RSD), indicating good reproducibility for the fluorescent chemosensor of  $Fe^{3+}$  ions.

The calculated LOD value of **L2** to detect  $Fe^{3+}$  ions was much lower compared with the permitted concentration of  $Fe^{3+}$  ions allowed in drinking water by the World Health Organization, that is 0.3 mg  $L^{-1}$  (~6 μM). This result indicated that **L2** could possibly be applied for the detection and quantification of  $Fe^{3+}$  ions from drinking water samples.<sup>[17]</sup> A comparison of LOD values for **L2** with other reported chemosensor agents is listed in Table 1 and compared with previous reports.<sup>[2,8,14–22,24,30,31,36–46]</sup> For comparison, the LOD value of **L2** was even better than pyrene, oxadiazole, coumarin, naphthalimide, quercetin, acridine, crown ether, triphenylamine, carbazole, rhodamine, triazole, and isatin derivatives. More than that, the sensing capability of **L2** was also better than hybrid inorganic/organic nanocomposite materials based on SBA-15 (see Table 1, entries

**TABLE 1** Comparison of fluorescent chemosensors for  $Fe^{3+}$  ions from the present work and previously reported studies

No	Ligand or compound	LOD (μM)	Solvent system	Reference
1	Pyrene–Schiff's base	3.19	DMSO:H <sub>2</sub> O (8:2)	[2]
2	Oxadiazole based	6.95	THF:Tris–HCl (4:1)	[8]
3	Pyrene–Schiff's base	1.37	DMSO:H <sub>2</sub> O (7:3)	[14]
4	Coumarin based	50.0	HEPES–1% DMSO	[15]
5	Naphthalimide dyes	2.00	THF:H <sub>2</sub> O (3:7)	[16]
6	Quercetin	20.5	DMSO:H <sub>2</sub> O (9:1)	[17]
7	Aminopyrine	1.82	THF	[18]
8	Acridine	4.13	DMSO:H <sub>2</sub> O (1:1)	[19]
9	Schiff's base–coumarin	4.30	MeOH	[20]
10	Schiff's base–crown ether	0.36	EtOH	[21]
11	Triphenylamine–Schiff's base	45.1	THF:H <sub>2</sub> O	[22]
12	Carbazole-based Schiff's base	3.62	CH <sub>3</sub> CN	[24]
13	Rhodamine–quinoline	0.83	MeOH	[30]
14	Naphthol–azo	0.94	CH <sub>3</sub> CN:H <sub>2</sub> O (1:1)	[31]
15	Rhodamine based	6.94	CH <sub>3</sub> CN:H <sub>2</sub> O (8:2)	[36]
16	Triazole derivative	3.21	Acetone:H <sub>2</sub> O (1:1)	[37]
17	Bis–rhodamine based	4.10	Methanol	[38]
18	Rhodamine–thioxoquinazoline	4.11	CH <sub>3</sub> CN:H <sub>2</sub> O (8:2)	[39]
19	Triazole–coumarin derivative	3.81	DMSO:H <sub>2</sub> O (n/a)	[40]
20	Naphthalimide–thiourea derivative	6.86	CH <sub>3</sub> CN:H <sub>2</sub> O (99:1)	[41]
21	Nanocomposite (SBA–15/isatin derivative)	0.60	H <sub>2</sub> O	[42]
22	Nanocomposite (SBA–15/bis–Schiff's base benzenediamine)	1.98	EtOH:H <sub>2</sub> O (9:1)	[43]
23	Diaza–18–crown–6 ether	0.31	DMF:H <sub>2</sub> O (4:1)	[44]
24	Quinoline based	0.16	DMSO:H <sub>2</sub> O (8:2)	[45]
25	Azo–Schiff's base anthranilic acid	6.44	DMF:HEPES (1:1)	[46]
26	Schiff's base–azo	0.31	H <sub>2</sub> O:MeOH (4:1)	Present work

21 and 22). This marked result indicated that chemosensor **L2** formed a suitable complexation of  $\text{Fe}^{3+}$  ions with its Schiff's base, phenolic, and azo moieties. It was known that Schiff's base and phenolic compounds had high sensitivity for  $\text{Fe}^{3+}$  detection.<sup>[21,31]</sup> By combining these functional groups with azo moieties, it was found that the LOD value of **L2** was lower than that of other hybrid compounds (see Table 1, entries 1, 9–12, and 25). In particular, compared with a quinoline-based chemosensor in DMSO:H<sub>2</sub>O (4:1),<sup>[45]</sup> our finding was almost that in aqueous system using MeOH:H<sub>2</sub>O (1:4) and was close to the lowest reported LOD value. Conversely, while the other chemosensor agents based on organic compounds required DMSO or THF as the diluent (Table 1), in the present work a commercially available solvent from the mixture of H<sub>2</sub>O:MeOH at 4:1 v/v volume ratio was used, which is relatively cheap and convenient.

This phenomenon has been also proved by investigating the sensitivity of **L1** for  $\text{Fe}^{3+}$  detection using fluorescence titration (Figure S7a,b) and Stern–Volmer plot for **L1** (Figure S8), yielding 2.49 and 8.29  $\mu\text{M}$  as the LOD and LOQ values, respectively. Interestingly, the LOD and LOQ values for **L2** were almost 10 times better than that for **L1**, confirming that the presence of an imine ( $-\text{C}=\text{N}$ ) functional group together with an azo ( $-\text{N}=\text{N}$ ) moiety was pivotal for chemosensor sensitivity. Indeed, the Stern–Volmer constant ( $K_{\text{SV}}$ ) was found to be  $2.43 \times 10^4 \text{ M}^{-1}$  from the calculation using Figure 4, which was relatively high due to the higher sensing capability of **L2** to be used as the chemosensor agent for detection of  $\text{Fe}^{3+}$  ions. The  $K_{\text{SV}}$  value of **L2** was higher than that of **L1** ( $7.50 \times 10^3 \text{ M}^{-1}$ ; Figure S8), indicating that the sensitivity of **L2** for  $\text{Fe}^{3+}$  detection was higher than that for **L1**.

### 3.3 | Investigation on the complex structure between **L2** and $\text{Fe}^{3+}$ ions

The stoichiometric ratio between **L2** and  $\text{Fe}^{3+}$  ions was further studied for interaction in the formation of a complex structure using a

Job's plot experiment. Job's plot was obtained from the intensity of the excitation signal at 233 nm, as shown in Figure 5a. It was found that the complex between **L2** and  $\text{Fe}^{3+}$  ions was formed in a 1:1 stoichiometric ratio. To support this result, Benesi–Hildebrand plots for **L1** and **L2** were constructed to calculate the association constant, as shown in Figures S9 and S10. In this case, the Benesi–Hildebrand plot was found to be linear, with 0.9921 as the correlation factor (Figure S10) to give an association constant for the  $[\text{L2-Fe}]^{3+}$  complex at  $1.56 \times 10^4 \text{ M}^{-1}$ . This result demonstrated a suitable 1:1 complexation interaction between **L2** and  $\text{Fe}^{3+}$  ions. The association constant for  $[\text{L2-Fe}]^{3+}$  was higher, around 22 times that of  $[\text{L1-Fe}]^{3+}$  in  $6.98 \times 10^2 \text{ M}^{-1}$  (Figure S9), demonstrating that the complexation ability of **L2** for binding  $\text{Fe}^{3+}$  ions was stronger than **L1**.

Furthermore, to discover the role for each functional group in the complex interaction between **L2** and  $\text{Fe}^{3+}$  ions, FTIR spectra for **L2** before and after the addition of  $\text{Fe}^{3+}$  ions were recorded, and the percentage quenching for each signal on the fluorescence titration study was also calculated, as shown in Figure 3d. After the addition of  $\text{Fe}^{3+}$  ions at 10 eq. to the ligand **L2**, the vibration peak corresponding to the imine ( $-\text{C}=\text{N}$ ) functional group was shifted from 1736 to 1715  $\text{cm}^{-1}$ . In addition, the vibration peak for the azo ( $-\text{N}=\text{N}$ ) functional group was shifted from 1401 to 1397  $\text{cm}^{-1}$ , while the vibration peak for C–O decreased its intensity as shown in Figure 5b. These results suggested that both  $-\text{C}=\text{N}$  and  $-\text{N}=\text{N}$  groups in **L2** were affected by the addition of  $\text{Fe}^{3+}$  ions, as strengthened by the significant quenching of the fluorescence spectra of **L2** with the addition of  $\text{Fe}^{3+}$  ions at 233 and 279 nm. The decrease in the vibration band for C–O indicated that the phenolic group ( $-\text{OH}$ ) adjacent to the azo group was also affected by the presence of  $\text{Fe}^{3+}$  ions.

As mentioned previously, the quenching percentages of excitation signals at 203, 233 and 279 nm could be assigned to aromatic, azo, and imine functional groups. The quenching percentages of excitation signals from aromatic, azo, and imine groups were increased at a nearly similar amount by increasing the concentration of  $\text{Fe}^{3+}$  ions,

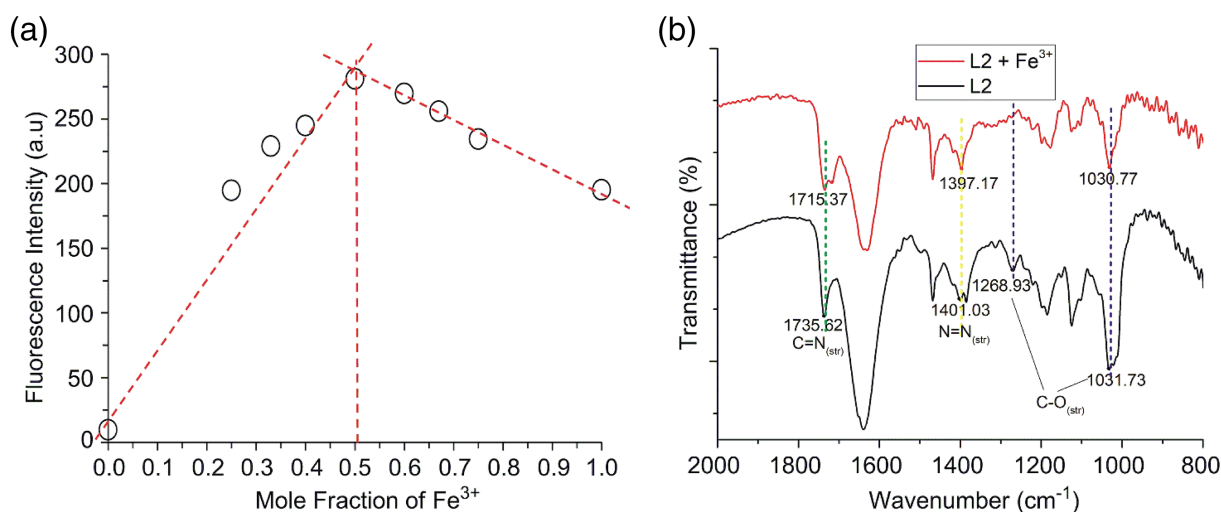


**FIGURE 5** (a) Job's plot of **L2** and  $\text{Fe}^{3+}$  ions in 30  $\mu\text{M}$ . (b) FTIR spectra of **L2** (30  $\mu\text{M}$ ) with and without the addition of  $\text{Fe}^{3+}$  ions at 10 eq. (300  $\mu\text{M}$ )

indicating that the three functional groups were affected during  $\text{Fe}^{3+}$  ion sensing. Considering the Job's plot result, this could only have occurred if the complex between **L2** with  $\text{Fe}^{3+}$  ions reacted in a 1:1 stoichiometric ratio through head-to-tail and tail-to-head interactions. Moreover, **L2** contains an azo group (adjacent to a hydroxyl group) and is electron rich (N atom), and could chelate well with an  $\text{Fe}^{3+}$  ion. The imine group was also considered to induce good chelation as it was rich in electrons.<sup>[26]</sup> As confirmed from the counteranion study, the hydroxyl group in **L2** was deprotonated due to the presence of  $\text{Fe}^{3+}$ . In addition, considering that the unfilled electrons in the d shell  $\text{Fe}^{3+}$  had strong paramagnetic properties, this could strongly affect the emission of a fluorophore unit through both electron or energy transfer to produce a quenching phenomenon.<sup>[47]</sup> Therefore, the

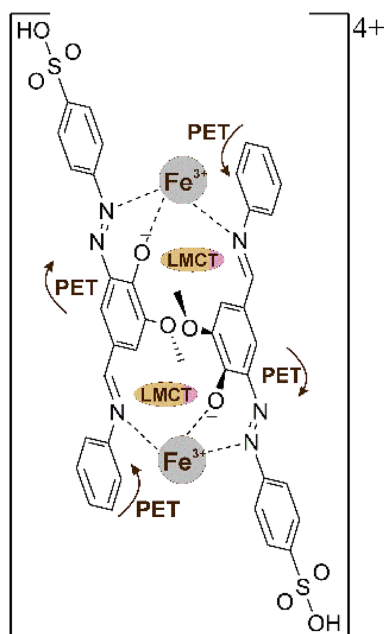


**FIGURE 6** Proposed complex formation for the interaction of **L2** and  $\text{Fe}^{3+}$  ions

fluorescence intensity of **L2** was gradually quenched by the addition of  $\text{Fe}^{3+}$  ions, and ligand–metal charge transfer (LMCT) could be the most plausible mechanism for supporting the quenching phenomenon. The paramagnetic properties of  $\text{Fe}^{3+}$  could immediately trigger the  $-\text{C}=\text{N}$  and  $-\text{N}=\text{N}$  groups to open a deactivation channel with non-radioactive properties, and tended to facilitate electron/energy transfer, causing fluorescence quenching to occur. This interaction could lead to photoinduced electron transfer (PET) of the aromatic ring near the azo and imine groups. Therefore, binding between **L2** with  $\text{Fe}^{3+}$  ions during molecular recognition<sup>[48]</sup> could induce the presence of both LMCT and PET (Figure 6). This formed complex could induce the quenching phenomenon with fluorescence properties from Turn-On to Turn-Off of its emission intensity, as shown in Scheme 1. Moreover, the interactions between  $\text{Fe}^{3+}$  ions and **L2** in this complex structure may be attributed to the ultrasensitive and selective detection of  $\text{Fe}^{3+}$  ions in  $\text{H}_2\text{O}:\text{MeOH}$  (4:1 v/v).

The effect of pH value on the  $\log[\text{Fe}^{3+}]$  (detected amount  $\text{Fe}^{3+}$  ions) as calculated from the standard curve is shown in Figure 7a. The plot between  $\Delta\text{pH}$  and  $\log[\text{Fe}^{3+}]$  (detected amount  $\text{Fe}^{3+}$  ions) produced a linear plot with a slope of  $y = 0.901x + 2.961$ , demonstrating that one proton of **L2** was exchanged during sensing of  $\text{Fe}^{3+}$  ions. Considering that **L2** has a phenolic group that would allow chelation with an azo functional group, this phenolic group plays an important role in  $\text{Fe}^{3+}$  sensing. As expected and shown in Figure 7b, there was no effect when using either chloride or citrate or sulfate as counteranions due to the ion-exchange mechanism in  $\text{Fe}^{3+}$  sensing. These results were well supported for the plausible mechanism as explained above (Figure 6).

### 3.4 | Selectivity study on $\text{Fe}^{3+}$ sensing in the presence of competitive metal ions

The selectivity study of  $\text{Fe}^{3+}$  sensing in the presence of other metal ions using **L2** was evaluated using other various metal ions such as  $\text{Na}^+$ ,  $\text{K}^+$ ,  $\text{Mg}^{2+}$ ,  $\text{Ca}^{2+}$ ,  $\text{Ba}^{2+}$ ,  $\text{Mn}^{2+}$ ,  $\text{Co}^{2+}$ ,  $\text{Cu}^{2+}$ ,  $\text{Ni}^{2+}$ ,  $\text{Zn}^{2+}$ , and  $\text{La}^{3+}$ .

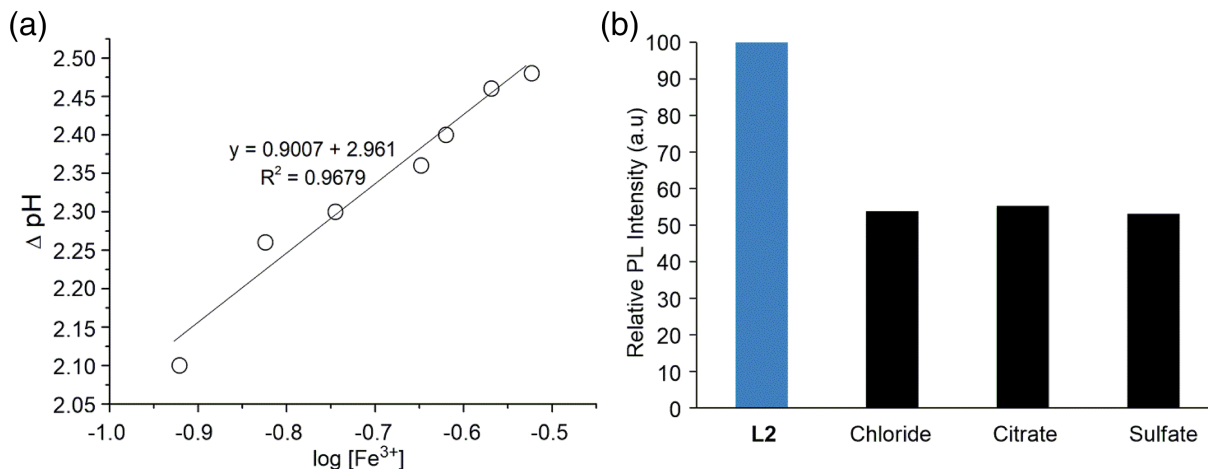


**FIGURE 7** (a) Plot of  $\Delta\text{pH}$  versus  $\log[\text{Fe}^{3+}]$ . (b) Counteranion effect of **L2** (30  $\mu\text{M}$ ) measured at emission 341 nm ( $\text{Fe}^{3+}$  ions in 1.0 eq.)



Figure 8 shows the fluorescence spectra of **L2** after the addition of various metal ions at 10 eq. to the concentration of **L2** (30  $\mu\text{M}$ ). Markedly,  $\text{Fe}^{3+}$  ions produced the quenching phenomenon only for the emission peak at 341 nm, while the other metal ions did not significantly change its initial emission intensity. Even though  $\text{La}^{3+}$  has the same positive charge as  $\text{Fe}^{3+}$  ions, **L2** produced no significant response toward  $\text{La}^{3+}$  that was as high as that for  $\text{Fe}^{3+}$  ions. This result indicated that **L2** is highly interactive only with  $\text{Fe}^{3+}$  ions to form the complex as mentioned above.

To evaluate the metal ion selectivity of **L2** in the quantitative amount, the interference percentage for the detection of  $\text{Fe}^{3+}$  ions with the presence of other competitive metal ions is shown in Table 2. The presence of other metal ions together with  $\text{Fe}^{3+}$  ions did not produce any significant interference (less than 2.5%) on  $\text{Fe}^{3+}$  ion quantification at 30  $\mu\text{M}$  concentration. This finding clearly demonstrated that **L2** is a promising candidate to be

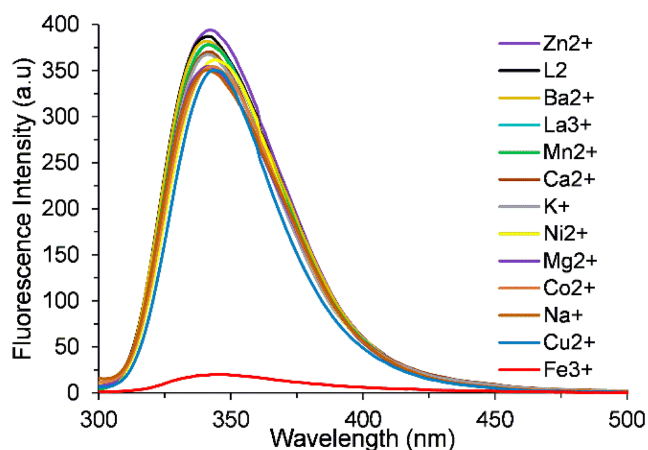


**FIGURE 8** Emission spectral changes of **L2** after the addition of various metal ions at the same concentrations

**TABLE 2** Interference percentage of  $\text{Fe}^{3+}$  ion sensing in the presence of other metal ions at 1.0 eq. ( $[\text{Fe}^{3+}] = 0.03 \text{ mM}$ )

Metal ions	Interference (%)
$\text{Na}^+$	0.09
$\text{K}^+$	0.09
$\text{Mg}^{2+}$	0.16
$\text{Ca}^{2+}$	0.70
$\text{Ba}^{2+}$	0.81
$\text{Mn}^{2+}$	0.86
$\text{Co}^{2+}$	0.52
$\text{Cu}^{2+}$	2.26
$\text{Ni}^{2+}$	1.54
$\text{Zn}^{2+}$	2.33
$\text{La}^{3+}$	1.08
All metal ions mixture	1.84

**TABLE 3**  $\text{Fe}^{3+}$  quantification from real water samples using **L2** through a spiking technique

Sample	$[\text{Fe}^{3+}] (\mu\text{M})$		Recovery (%)
	Before spiking	After spiking	
Tap water	15.12	30.75	102
Drinking water A	13.04	30.19	107

used as a chemosensor agent with high selectivity for detection of  $\text{Fe}^{3+}$  ions in real sample analysis.

**L2** was used to quantify  $\text{Fe}^{3+}$  ions from tap and commercially available drinking water and evaluate its potential for real applications. The recovery percentage was calculated based on spiking with 15  $\mu\text{M}$   $\text{Fe}^{3+}$  ions as a standard solution. As shown in Table 3, **L2** gave 102–107% recovery percentages, which was really good enough for such simple chemosensors. Moreover, three replicate measurements for each real sample displayed an RSD of less than 3%, indicating good reproducibility of **L2** to be used as a fluorescent chemosensor agent for quantification of  $\text{Fe}^{3+}$  ions in real aquatic samples. Because of that, this novel **L2** probe is a promising chemosensor to be developed for fluorescence detection of toxic elements and dangerous pollutants such as lead ions with high selectivity, including with their simple portable analytical devices.<sup>[49,50]</sup>

## 4 | CONCLUSION

From the results, it was found that **L2** as a fluorescent chemosensor could selectively detect and quantify  $\text{Fe}^{3+}$  ions through a significant quenching phenomenon up to 100% at its emission signal at 341 nm. The LOD and LOQ values were 0.31 and 1.04  $\mu\text{M}$ , which is much lower than the permitted maximum  $\text{Fe}^{3+}$  ion concentration in drinking water as stated by the recent government regulation and shows ultrasensitive detection so far in aqueous systems. Such an increment of **L2** sensing capability is due to the presence of the imine group together with the azo functional groups. Moreover, the complexation study between  $\text{Fe}^{3+}$  ions and **L2** was performed using Job's plot and Benesi–Hildebrand equation, and it was found that **L2** and  $\text{Fe}^{3+}$  ions could form a 1:1 complex with  $1.56 \times 10^4 \text{ M}^{-1}$  value as the association constant. From the interference test, it clearly showed that there was no significant interference from other metal ions towards sensing  $\text{Fe}^{3+}$  ion with **L2**. These findings may also shed light on the practical issues for the development of **L2** as a water-soluble and a selective fluorescent chemosensor of  $\text{Fe}^{3+}$  ions, in which excellent chemosensors could be potentially applied for water monitoring in real time.

## ACKNOWLEDGEMENTS

This research was supported by the Ministry of Research, Technology, and Higher Education, The Republic of Indonesia through a Fundamental Research Grant (Penelitian Dasar) 2019 with agreement no. 009/MACHUNG/LPPM/SP2H-LIT-MULTI/III/2019.

## ORCID

Krisfian Tata Aneka Priyanga  <https://orcid.org/0000-0002-4119-2470>

Yehezkiel Steven Kurniawan  <https://orcid.org/0000-0002-4547-239X>

Leny Yuliati  <https://orcid.org/0000-0003-1600-5757>

Bambang Purwono  <https://orcid.org/0000-0001-6284-7782>

Tutik Dwi Wahyuningsih  <https://orcid.org/0000-0001-5741-2848>

Hendrik O. Lintang  <https://orcid.org/0000-0002-1911-8100>

## REFERENCES

- [1] K. S. Sista, S. Dwarapudi, *ISIJ Int.* **2018**, *58*, 999.
- [2] Y. R. Bhorge, H. T. Tsai, K. F. Huang, A. J. Pape, S. N. Janaki, Y. P. Yen, *Spectrochim. Acta A Mol. Biomol. Spectrosc.* **2014**, *130*, 7.
- [3] C. Wang, D. Zhang, X. Huang, P. Ding, Z. Wang, Y. Zhao, Y. Ye, *Talanta* **2014**, *128*, 69.
- [4] C. Brugnara, *Clin. Chem.* **2003**, *49*, 1573.
- [5] S. N. Nandeshwar, A. S. Mahakalakar, R. R. Gupta, G. Z. Kyzas, *J. Mol. Liq.* **2016**, *216*, 688.
- [6] C. Zhang, M. Wang, Y. Zhang, Z. Li, S. Xu, *Instrum. Sci. Technol.* **2017**, *46*, 292.
- [7] A. Rabajczyk, J. Namieśnik, *Water Environ. Res.* **2014**, *86*, 741.
- [8] X. Gong, H. Zhang, N. Jiang, L. Wang, G. Wang, *Microchem. J.* **2019**, *145*, 435.
- [9] J. Hua, Y. G. Wang, *Chem. Lett.* **2005**, *34*, 98.
- [10] D. Vlasici, E. Fagadar-Cosma, E. Popa, V. Chiriac, M. Gil-Agusti, *Sensors* **2012**, *12*, 8193.
- [11] A. H. Ja-an, C. Heng-Chia, S. Wen-Ta, *Anal. Chem.* **2012**, *84*, 3246.
- [12] L. Huang, F. Hou, J. Cheng, P. Xi, F. Chen, D. Bai, Z. Zeng, *Org. Biomol. Chem.* **2012**, *10*, 9634.
- [13] Y. Z. Chen, Y. R. Bhorge, A. J. Pape, R. D. Divate, Y. C. Chung, Y. P. Yen, *J. Fluoresc.* **2015**, *25*, 1331.
- [14] O. García-Beltrán, B. Cassels, C. Pérez, N. Mena, M. Núñez, N. Martínez, M. Aliaga, *Sensors* **2014**, *14*, 1358.
- [15] H. Jia, X. Gao, Y. Shi, N. Sayyadi, Z. Zhang, Q. Zhao, R. Zhang, *Spectrochim. Acta A Mol. Biomol. Spectrosc.* **2015**, *149*, 674.
- [16] E. Normaya, M. Fazli, M. Norazmi Ahmad, K. H. K. Bulat, *J. Mol. Struct.* **2019**, *1184*, 538.
- [17] E. Şenkuytu, *Inorg. Chim. Acta* **2017**, *479*, 58.
- [18] C. Wang, J. Fu, K. Yao, K. Xue, K. Xu, X. Pang, *Spectrochim. Acta A Mol. Biomol. Spectrosc.* **2018**, *199*, 403.
- [19] L. Wang, H. Li, D. Cao, *Sensor Actuat. B Chem.* **2013**, *181*, 749.
- [20] G. Dong, K. Duan, Q. Zhang, Z. Liu, *Inorg. Chim. Acta* **2019**, *487*, 322.
- [21] M. R. G. Fahmi, A. T. N. Fajar, N. Roslan, L. Yuliati, A. Fadlan, M. Santoso, H. O. Lintang, *Open Chem.* **2019**, *17*, 438.
- [22] L. J. Fan, Y. Zhang, C. B. Murphy, S. E. Angell, M. F. L. Parker, B. R. Flynn, W. E. Jones, *Coord. Chem. Rev.* **2009**, *253*, 410.
- [23] Z. X. Li, W. Zhou, L. F. Zhang, R. L. Yuan, X. J. Liu, L. H. Wei, M. M. Yu, *J. Lumin.* **2013**, *136*, 141.
- [24] L. Yang, W. Zhu, M. Fang, Q. Zhang, C. Li, *Spectrochim. Acta A Mol. Biomol. Spectrosc.* **2013**, *109*, 186.
- [25] Z. X. Li, L. F. Zhang, W. Y. Zhao, X. Y. Li, Y. K. Guo, M. M. Yu, J. X. Liu, *Inorg. Chem. Commun.* **2011**, *14*, 1656.
- [26] A. Khedr, M. Gaber, R. Issa, H. Erten, *Dyes Pigm.* **2005**, *67*, 117.
- [27] A. L. Berhanu, G. Gaurav, I. Mohiuddin, A. K. Malik, J. S. Aulakh, V. Kumar, K. H. Kim, *TrAC, Trends Anal. Chem.* **2019**, *116*, 74.
- [28] A. M. Abu-Dief, I. M. A. Mohamed, *Beni-Suef Univ. J. Basic Appl. Sci.* **2015**, *4*, 119.
- [29] A. M. Costero, S. Gil, M. Parra, P. M. E. Mancini, M. N. Kneeteman, M. I. Quindt, *Tetrahedron Lett.* **2015**, *56*, 3988.
- [30] J. Qin, Z. Yang, G. Wang, *J. Photochem. Photobiol. A* **2015**, *310*, 122.
- [31] A. Panja, K. Ghosh, *Mater. Chem. Front.* **2018**, *2*, 1.
- [32] H. Khanmohammadi, M. Darvishpour, *Dyes Pigm.* **2009**, *81*, 167.
- [33] M. J. Reimann, D. R. Salmon, J. T. Horton, E. C. Gier, L. R. Jefferies, *ACS Omega* **2019**, *4*, 2874.
- [34] L. Zhou, P. Cai, Y. Feng, J. Cheng, H. Xiang, J. Liu, D. Wu, X. Zhou, *Anal. Chim. Acta* **2012**, *735*, 96.
- [35] K. Hamidian, M. Irandoust, E. Rafiee, M. Joshaghani, *Z. Naturforsch. B* **2012**, *67(2)*, 159.
- [36] P. S. Nayab, M. Shkir, *Sensor Actuat. B Chem.* **2017**, *245*, 395.
- [37] K. Shah, N. ul. Ain, F. Ahmed, I. Anis, M. R. Shah, *Sensor Actuat. B Chem.* **2017**, *249*, 515.
- [38] L. He, C. Liu, J. H. Xin, *Sensor Actuat. B Chem.* **2015**, *213*, 181.
- [39] Y. Wang, H. Q. Chang, W. N. Wu, X. L. Zhao, Y. Yang, Z. Q. Xu, L. Jia, *Sensor Actuat. B Chem.* **2017**, *239*, 60.
- [40] T. Puthiyedath, D. Bahulayan, *Sensor Actuat. B Chem.* **2018**, *272*, 110.
- [41] Z. Zhang, S. Lu, C. Sha, D. Xu, *Sensor Actuat. B Chem.* **2015**, *208*, 258.
- [42] N. Lashgari, A. Badiiei, G. M. Ziarani, *J. Phys. Chem. Solids* **2017**, *103*, 238.
- [43] J. Q. Wang, L. Huang, M. Xue, Y. Wang, L. Gao, J. H. Zhu, Z. Zou, *J. Phys. Chem. C* **2008**, *112*, 5014.
- [44] H. Li, L. Li, B. Yin, *Inorg. Chem. Commun.* **2014**, *42*, 1.
- [45] P. Madhu, P. Sivakumar, *J. Mol. Struct.* **2019**, *1193*, 378.
- [46] O. Ozdemir, *Turk. J. Chem.* **2019**, *43*, 266.
- [47] W. He, Z. Liu, *RSC Adv.* **2016**, *6*, 59073.
- [48] Z. Li, L. Zhang, X. Li, Y. Guo, Z. Ni, J. Chen, M. Yu, *Dyes Pigm.* **2012**, *94*, 60.
- [49] C. V. Nguyen, W. H. Chiang, K. C. W. Wu, *Bull. Chem. Soc. Jpn.* **2019**, *92*, 1430.
- [50] H. Wang, L. Yang, S. Chu, B. Liu, Q. Zhang, L. Zou, S. Yu, C. Jiang, *Anal. Chem.* **2019**, *91*, 9292.

## SUPPORTING INFORMATION

Additional supporting information may be found online in the Supporting Information section at the end of this article.

**How to cite this article:** Priyanga KTA, Kurniawan YS, Yuliati L, Purwono B, Wahyuningsih TD, Lintang HO. Novel luminescent Schiff's base derivative with an azo moiety for ultraselective and sensitive chemosensor of Fe<sup>3+</sup> ions. *Luminescence*. 2021;36:1239–1248. <https://doi.org/10.1002/bio.4049>

**LUMINESCENCE**  
The Journal of Photophysics and Photochemistry



Volume 10

WILEY




## Editorial Board


### Editor-in-Chief

 **Prof Xinrong Zhang**, Analysis Center, Department of Chemistry, Tsinghua University, Beijing 100084, PR China  
E-mail: [xrzhang@mail.tsinghua.edu.cn](mailto:xrzhang@mail.tsinghua.edu.cn)

### Associate Editor-in-Chief

 **Prof Aldo Roda**, Department of Chemistry G. Ciamician, Alma Mater Studiorum-University of Bologna Via Selmi 2, 40126 Bologna, Italy  
E-mail: [aldo.roda@unibo.it](mailto:aldo.roda@unibo.it)

### Editors

 **Prof Ana M. García-Campaña**, University of Granada, Granada, Spain

 **Prof Philippe Giamarchi**, Université Européenne de Bretagne, Brest, France

 **Dr Sanjay J. Dhoble**, R.T.M. Nagpur University, Nagpur, India

 **Prof Jin-Ming Lin**, Tsinghua University, Beijing, China

 **Prof Yi Lv**, Sichuan University, Chengdu, China

 **Prof Yoshihiro Ohmiya**, BioMedical Research Institute, Japan

### Founding Editors

 **Prof L. K. Kricka**, USA

 **Dr P. E. Stanley**, UK

### Editorial Board


 **Prof H.Y. Aboul-Enein**, National Research Center, Cairo, Egypt

 **Prof Phil Hill**, University of Nottingham, Loughborough, UK

 **Prof Wilhelm Josef Baader**, Universidade de Sao Paulo, Sao Paulo, Brazil

 **Dr Jerome Mallefet**, Université Catholique de Louvain, Louvain-de-Neuve, Belgium

 **Prof W.R.G. Baeyens**, *University of Ghent, Belgium*

 **Prof A.A. Szalay**, *University of Wurzburg, Wurzburg, Germany*

 **Prof A.K. Campbell**, *University of Wales, Cardiff, UK*

 **Dr Dieter Weiss**, *Freidrich Schiller Universitat, Jena, Germany*

 **Dr S.H.D. Haddock**, *Monterey Bay Aquariam Research Institute California, California, USA*

#### Ex Officio Editorial Board Members

 **Professor T. Lövgren**, *University of Turku, Turku, Finland*

 **Prof. Zachary Schultz**, *University of Notre Dame, Indiana, USA*

#### Publisher

**Charlotte Liu**, *Wiley*

#### More from this journal

- [Wiley Job Network](#)
- [See Your Article on the Cover](#)

### About Wiley Online Library

[Privacy Policy](#)

[Terms of Use](#)

[Cookies](#)

[Accessibility](#)

[Help & Support](#)

[Contact Us](#)

[DMCA & Reporting Piracy](#)

[Opportunities](#)

[Subscription Agents](#)

[Advertisers & Corporate Partners](#)

[Connect with Wiley](#)

[The Wiley Network](#)

[Wiley Press Room](#)



Volume 36, Issue 5

Pages: 1107-1340  
August 2021

< Previous Issue | Next Issue >

GO TO SECTION

Submit an article

Browse free sample issue

Get Content alerts

Subscribe to this journal

More from this journal

- Call for Papers: Special Issue on Smart and intelligent optical materials for sensing applications
- Wiley Job Network
- See Your Article on the Cover

Export Citation(s)

## ISSUE INFORMATION

Free Access

Issue Information

Pages: 1107-1109 | First Published: 06 July 2021

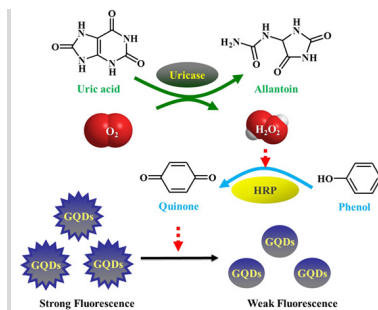
Abstract | PDF | Request permissions

## RESEARCH ARTICLES

### Enzyme-coupled fluorescence sensor for sensitive determination of uric acid and uricase inhibitor

Yuan Jiao, Yunlong Xing, Kai Li, Zainan Li, Guoqing Zhao

Pages: 1110-1116 | First Published: 24 July 2020



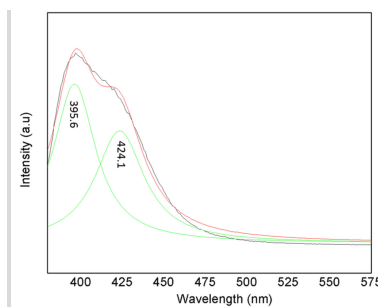
An enzyme-coupled fluorescence sensor was developed for the sensitive detection of uric acid and uricase inhibitor based on graphene quantum dots.

Abstract | Full text | PDF | References | Request permissions

### Structural and optical characterizations of Ce<sup>3+</sup>-doped YSO phosphors via the addition of TEOS

Seyed Mahdi Rafiaei, Mohammadreza Shokouhimehr

Pages: 1117-1123 | First Published: 17 December 2020



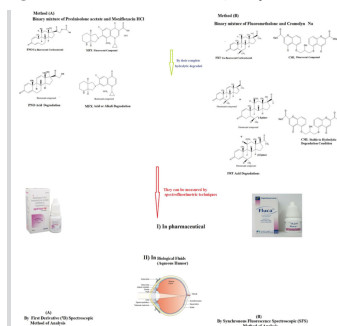
In this investigation, it was found that within the sol-gel method, YSO compounds including  $Y_{4.67}(SiO_4)_3O$ ,  $Y_2Si_2O_7$ , and  $Y_2SiO_5$  possessed the strongest photoluminescence characteristics.

Abstract | Full text | PDF | References | Request permissions

### Selective spectrofluorimetric determination of two corticosteroids along with their co-formulated drugs and degradation products in ophthalmic solution and aqueous humour

May H. Abdelwahab, Maha A. Hegazy, Soheir A. Weshahy, Hassan A.M. Hendawy, Samah S. Abbas

Pages: 1124-1142 | First Published: 11 January 2021



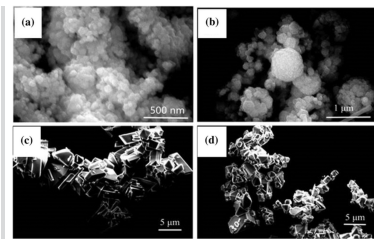
Accurate, specific, and cheap stability-indicating spectrofluorimetric methods were performed for two nonfluorescent corticosteroids without derivatization, each in the presence of their co-formulated drug and degradation products. Efficient spectrofluorimetric resolution of the studied binary mixtures and their degradation products was achieved. Factors affecting fluorescence were studied and these methods were validated according to ICH guidelines. Analysis of the biological parameters and validation using United States Food and Drug Administration bioanalytical validation guidelines was performed.

Abstract | Full text | PDF | References | Request permissions

### Crystal phase, morphology evolution and luminescence properties of Eu<sup>3+</sup>-doped BiPO<sub>4</sub> phosphor prepared using the hydrothermal method

Dongyan Yu, Xingya Wu, Gongqin Yan, Jieliang Cao

Pages: 1143-1150 | First Published: 05 March 2021



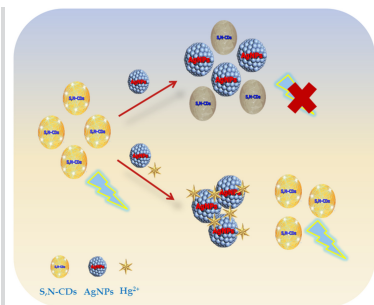
A series of Bi<sub>1-x</sub>Eu<sub>x</sub>PO<sub>4</sub> phosphors with controllable morphologies and desirable size was successfully prepared using an easy citric acid-assisted hydrothermal method.

[Abstract](#) | [Full text](#) | [PDF](#) | [References](#) | [Request permissions](#)

### A sensitive turn-off-on fluorometric sensor based on S,N co-doped carbon dots for environmental analysis of Hg(II) ion

Zahra Abolghasemi-Fakhri, Tooba Hallaj, Mohammad Amjadi

Pages: 1151-1158 | First Published: 08 March 2021



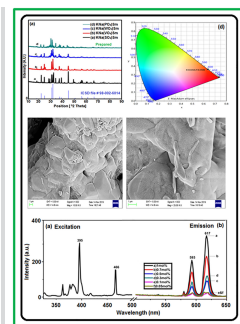
A simple and sensitive fluorescence turn-off-on sensor was established by S,N-CDs and AgNPs for determination of Hg<sup>2+</sup>.

[Abstract](#) | [Full text](#) | [PDF](#) | [References](#) | [Request permissions](#)

### Solid state diffusion and amalgamating anionic exchange at a KNaSO<sub>4</sub> phosphors activated with Eu<sup>3+</sup>, Dy<sup>3+</sup> and Sm<sup>3+</sup> rare earth ions to enhance w-LED performance

Arati Duragkar, Nirupama S. Dhoble, Ritesh L. Kohale, Sanjay J. Dhoble

Pages: 1159-1171 | First Published: 08 March 2021



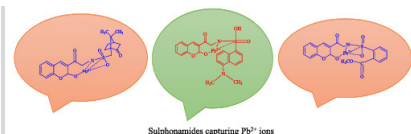
Rare earth KNaSO<sub>4</sub> phosphor doped with Eu<sup>3+</sup>, Dy<sup>3+</sup> and Sm<sup>3+</sup> were synthesized by solid state diffusion. KNaSO<sub>4</sub> phosphor doped with Eu<sup>3+</sup>, Dy<sup>3+</sup> and Sm<sup>3+</sup> ions were characterized by XRD, PL, SEM and FTIR.

[Abstract](#) | [Full text](#) | [PDF](#) | [References](#) | [Request permissions](#)

### Pb<sup>2+</sup> sensing by coumarin sulphonamide hybrids in aqueous medium

Nidhi Sharma, Ashu Gulati

Pages: 1172-1180 | First Published: 13 March 2021



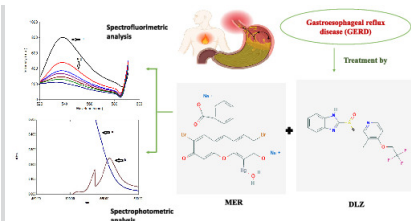
The sulphonamide substituted coumarin chromophores capturing toxic Pb<sup>2+</sup> ions by offering selectivity in binding positions. The receptors strikingly chelate Pb<sup>2+</sup> by exhibiting *hard borderline soft* acid base interactions with them in aqueous medium.

[Abstract](#) | [Full text](#) | [PDF](#) | [References](#) | [Request permissions](#)

### New spectroscopic methods for determination of dexlansoprazole using mercurochrome

Aya Roshdy, Heba Elmansi, Shereen Shalan, Amina El-Brashy

Pages: 1181-1188 | First Published: 16 March 2021



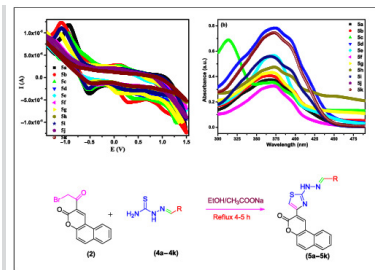
Dexlansoprazole is proton pump inhibitor that reacts with ion pairing agents such as Mercurochrome at pH 3.7. Measurement of the developed binary complex (spectrophotometric method) or the Mercurochrome quenching effect of the drug (spectrofluorimetric method) was carried out to establish rapid, easy, sensitive, and green methods to estimate levels of the studied drug either in its pure form or in pharmaceutical formulations.

[Abstract](#) | [Full text](#) | [PDF](#) | [References](#) | [Request permissions](#)

### Effect of organic solvents on solvatochromic, fluorescence, and electrochemical properties of synthesized thiazolycoumarin derivatives

Ali Bahadur, Shahid Iqbal, Rabail Ujan, Pervaiz Ali Channar, Murefah Mana AL-Anazy, Amer Saeed, Qaiser Mahmood, Muhammad Shoaib, Mazloom Shah, Ifzan Arshad, Ghulam Shabir, Muhammad Saifullah, Guocong Liu, Muhammad Abdul Qayyum

Pages: 1189-1197 | First Published: 23 March 2021



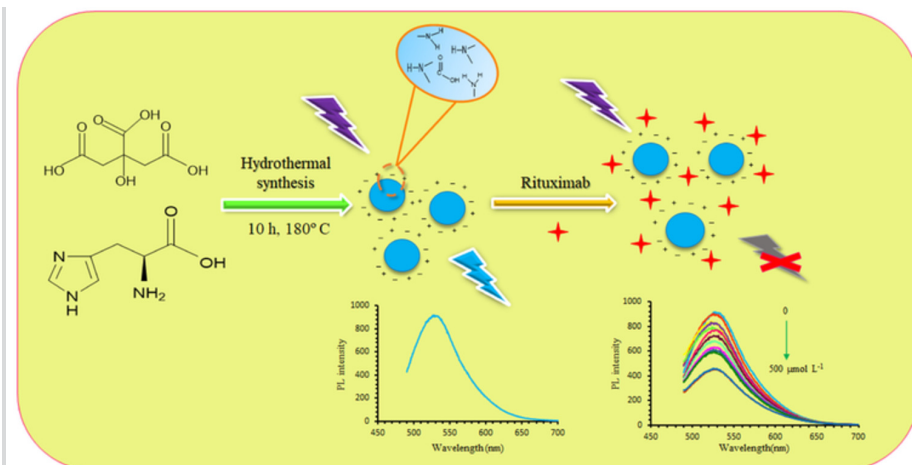
In this present investigation, novel thiazolycoumarins were synthesized by a multistep route. Thiazolycoumarins showed the solvatochromic effect in fluorescence and absorbance.

Abstract | Full text | PDF | References | Request permissions

### pH-responsive zwitterionic carbon dots for detection of rituximab

Elham Emami, Mohammad H. Mousazadeh

Pages: 1198-1208 | First Published: 22 March 2021



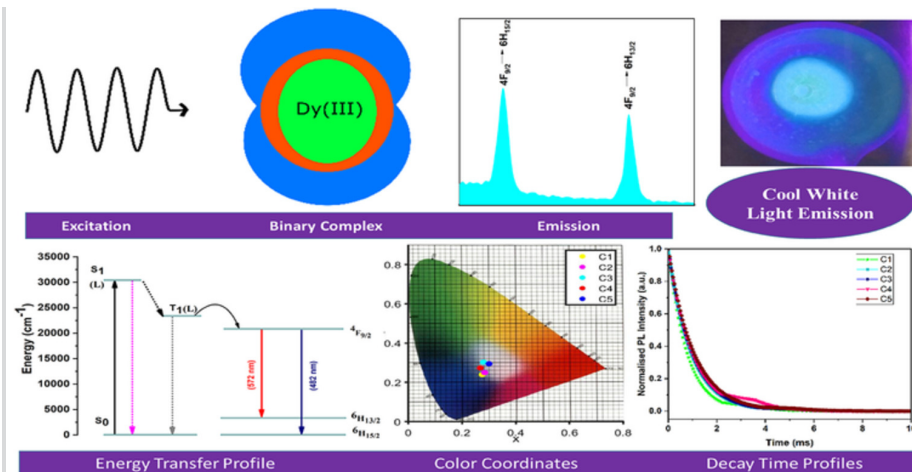
Schematic illustration of the synthesis of zwitterionic CDs for detection of rituximab.

Abstract | Full text | PDF | References | Request permissions

### Synthesis of cool white light emitting novel dysprosium (Dy<sup>3+</sup>) complexes with tetradentate β-ketoamide and heterocyclic auxiliary ligands

Monika Punia, Satyender Pal Khatkar, Vinod Bala Taxak, Priyanka Dhanekar, Priti Boora Doon

Pages: 1209-1219 | First Published: 29 March 2021



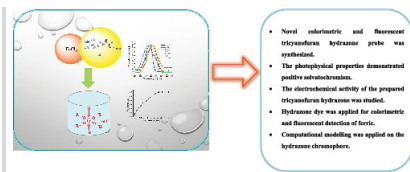
In this research work we reported a novel series of five complexes consisting of one binary and four ternary complexes that emitted cool white light and that were successfully synthesized using chelating tetradentate ligand and auxiliary ligands. The complexes were analyzed systematically by different techniques. Photoluminescence studies as well as colour purity and correlated colour temperature values confirmed cool white emission of the complexes in visible region. The energy transfer mechanism confirmed effective complexation of ligands with metal ions.

Abstract | Full text | PDF | References | Request permissions

### Synthesis and characterization of novel tricyanofuran hydrazone probe: solvatochromism, density-functional theory calculation and selective fluorescence, and colorimetric determination of iron (III)

Amal Al-Azmi, Elizabeth John

Pages: 1220-1230 | First Published: 31 March 2021



- Novel colorimetric and fluorescent tricyanofuran hydrazone probe was synthesized.
- The photophysical properties demonstrated positive solvatochromism.
- The electrochemical activity of the prepared tricyanofuran hydrazone was studied.
- Hydrazone dye was applied for colorimetric and fluorescent detection of iron.
- Computational modelling was applied on the hydrazone chromophore.



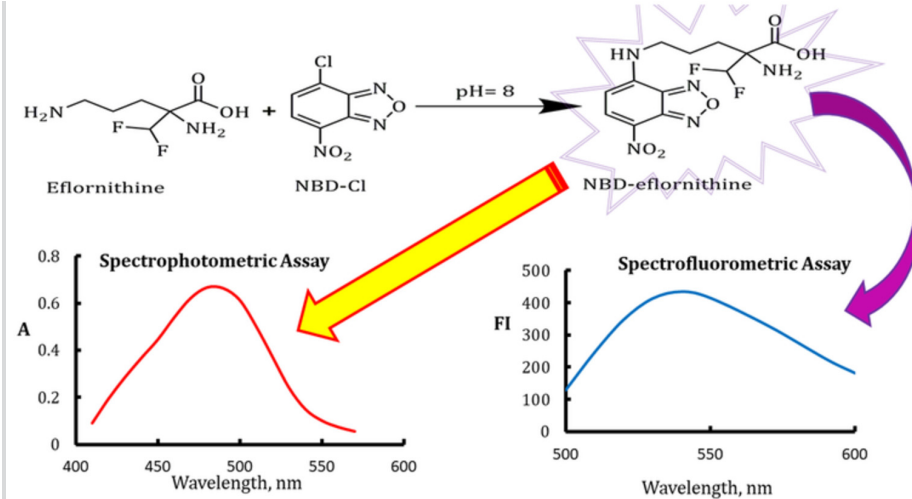
• Novel colorimetric and fluorescent tricyanofuran hydrazone probe was synthesized. • The photophysical properties demonstrated positive solvatochromism. • The electrochemical activity of the prepared tricyanofuran hydrazone was studied. • Hydrazone dye was applied for colorimetric and fluorescence detection of ferric. • Computational modelling was applied on the hydrazone chromophore.

Abstract | Full text | PDF | References | Request permissions

### Utility of 4-chloro-7-nitrobenzofuran for spectrofluorimetric and spectrophotometric determinations of the anti-hirsutism agent ( $\alpha$ -difluoromethylornithine) in pharmaceutical cream samples

Albandary Almahri

Pages: 1231-1238 | First Published: 05 April 2021



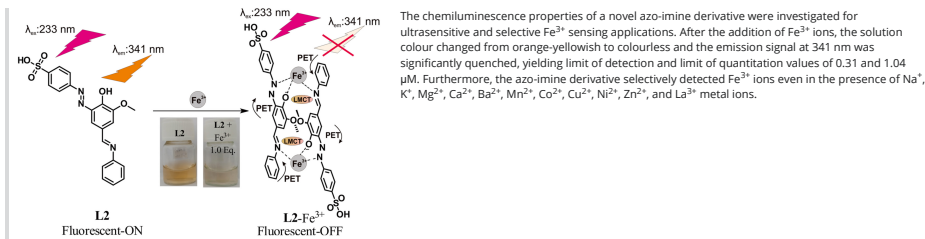
Spectrofluorometric and spectrophotometric determination of  $\alpha$ -difluoromethylornithine after its derivatization with 4-chloro-7-nitrobenzofuran (NBD-chloride) reagent.

Abstract | Full text | PDF | References | Request permissions

### Novel luminescent Schiff's base derivative with an azo moiety for ultrasensitive and sensitive chemosensor of $Fe^{3+}$ ions

Krisfian Tata Aneka Priyanga, Yehezkiel Steven Kurniawan, Leny Yulianti, Bambang Purwono, Tutik Dwi Wahyuningsih, Hendrik O. Lintang

Pages: 1239-1248 | First Published: 08 April 2021

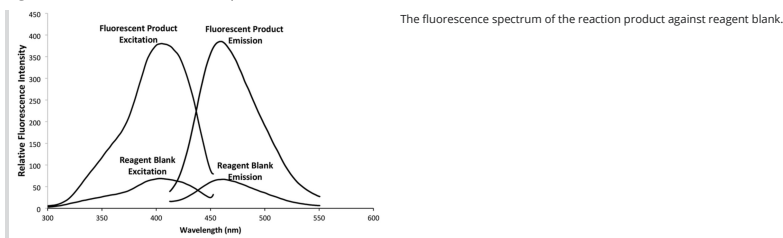


Abstract | Full text | PDF | References | Request permissions

### The first spectrofluorimetric approach for quantification of colistin sulfate and its prodrug colistimethate sodium in pharmaceutical dosage form and human plasma

Khalid M. Badr El-Din, Mahmoud A. Abdelmajed, Mahmoud A. Omar, Tamer Z. Attia

Pages: 1249-1256 | First Published: 12 April 2021

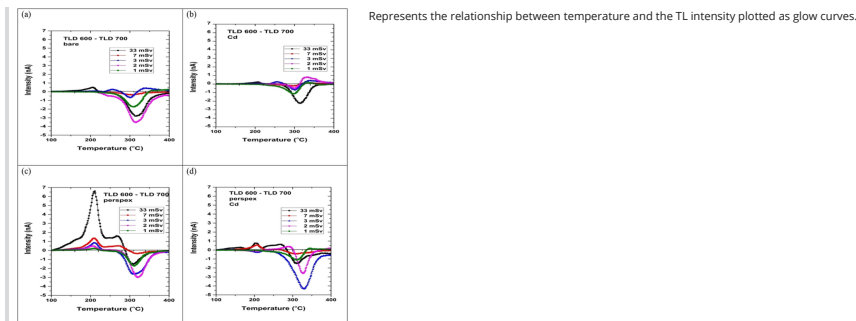


Abstract | Full text | PDF | References | Request permissions

### Response of TLD-600/TLD-700 and CR-39 to neutrons for medical dosimetry

Nabil El-Faramawy, Vibha Chopra, Shrouk Rawash, Arafah Abd El-Hafez, Sanjay J. Dhoble

Pages: 1257-1264 | First Published: 09 April 2021

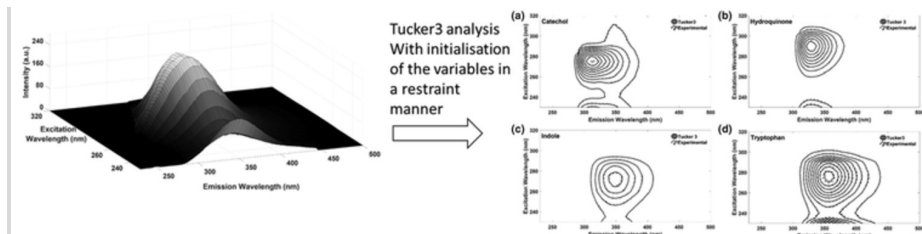


Abstract | Full text | PDF | References | Request permissions

## Tucker3 modelling of EEMF spectroscopic data sets using restrained initialization of spectral variables: fluorimetric analysis of mixtures consisting of bioactive molecules

Keshav Kumar

Pages: 1265-1271 | First Published: 09 April 2021



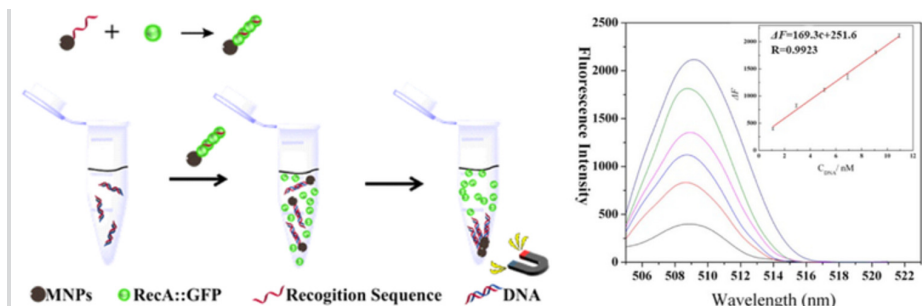
The present work introduces a novel spectral initialization approach to fit the Tucker3 model to EEMF spectroscopic data sets of dilute aqueous mixture of bioactive molecules.

[Abstract](#) | [Full text](#) | [PDF](#) | [References](#) | [Request permissions](#)

## Simple and sensitive detection of deoxyribonucleic acid using a RecA-GFP fusion protein-DNA filament as probe

Zijing Ren, Yuanfu Zhang, Tao Wu, Qingwang Xue, Shuhao Wang

Pages: 1272-1276 | First Published: 10 April 2021



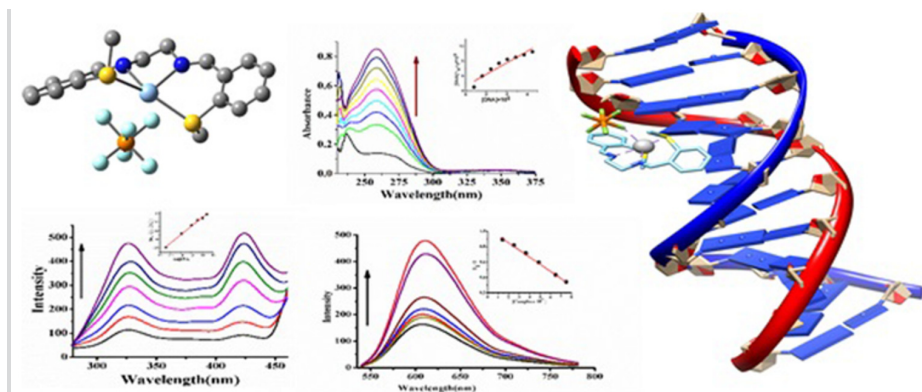
- A simple, rapid and highly sensitive method for the detection of double-stranded DNA (dsDNA) was developed using the RecA-ssDNA filament.
- This method presented high sensitive which could detect dsDNA as low as 0.12 nM, since the recombination of one chain DNA could release several RecA-GFP fusion proteins to amplify the fluorescence signal.
- Compared with the conventional methods, This method has the advantages of simple operation, high specificity and high sensitivity.

[Abstract](#) | [Full text](#) | [PDF](#) | [References](#) | [Request permissions](#)

## In vitro investigation of biophysical interactions between Ag(I) complexes of bis(methyl)(thia/selena)salen and ct-DNA via multi-spectroscopic, physicochemical and molecular docking methods along with cytotoxicity study

Mamta Tripathi, Rabbani Syed, Antony Stalin, Abdul Malik, Rama Pande, Ashish K. Asatkar

Pages: 1277-1284 | First Published: 09 April 2021



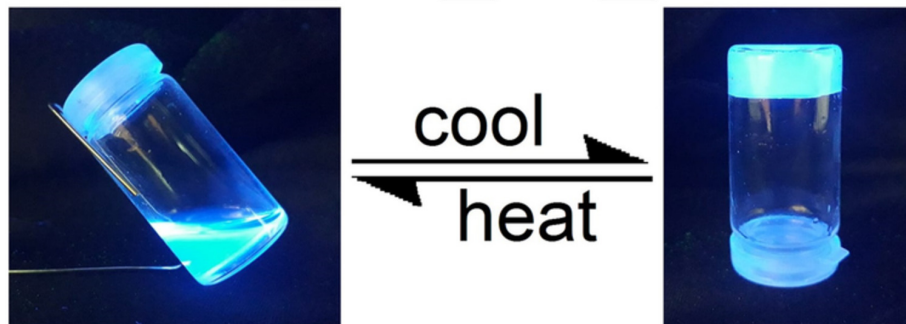
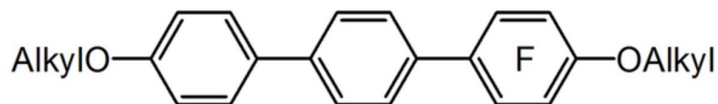
Four silver(I) complexes; **1**.PF<sub>6</sub>, **2**.PF<sub>6</sub>, **1**.ClO<sub>4</sub> and **2**.ClO<sub>4</sub> of bis(methyl)thia salen (**1**) and bis(methyl)selena salen (**2**) with two different counter anions (PF<sub>6</sub><sup>-</sup> and ClO<sub>4</sub><sup>-</sup>) have been investigated for DNA binding properties. Both experimentation and theoretical calculations were done to obtain an insight into the binding mechanism. The results obtained from both studies show good correlation.

[Abstract](#) | [Full text](#) | [PDF](#) | [References](#) | [Request permissions](#)

## Synthesis and characterization of novel fluoroterphenyls: self-assembly of low-molecular-weight fluorescent organogel

Naif Ghazi Altom

Pages: 1285-1299 | First Published: 14 April 2021



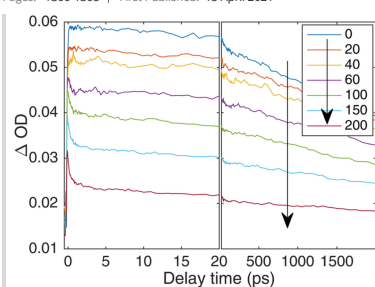
Application of nucleophilic aromatic substitution chemistry and CuI-catalyzed decarboxylative cross-coupling for the synthesis of fluorescent *para* alkoxy-functionalized fluorinated terphenyls based low molecular weight organogels.

[Abstract](#) | [Full text](#) | [PDF](#) | [References](#) | [Request permissions](#)

#### Ultrafast dynamics on fluorescence quenching of rhodamine 6G by graphene oxide

Dunli Liu, Qiuyun Wang, Anmin Chen, Qingyi Li, Laizhi Sui, Mingxing Jin

Pages: 1300-1305 | First Published: 15 April 2021



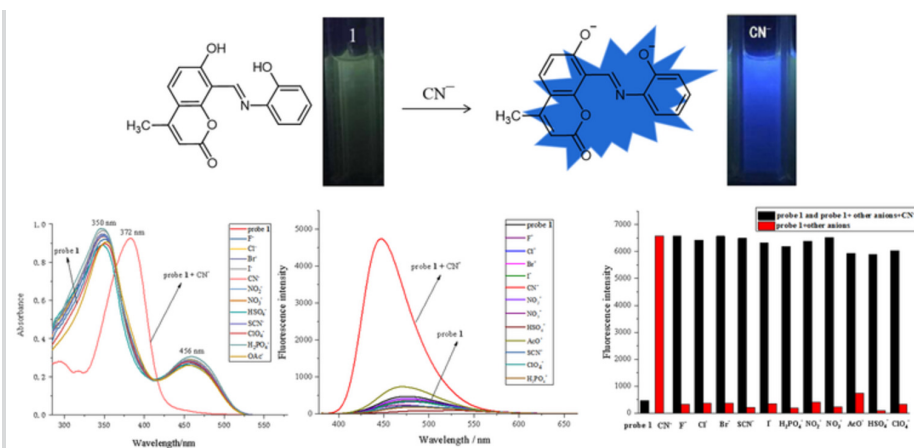
Ultrafast time-resolved absorption spectroscopy shows that there is a new transition process (electron transfer) in the excited rhodamine 6G and GO aqueous solution.

[Abstract](#) | [Full text](#) | [PDF](#) | [References](#) | [Request permissions](#)

#### A dual-channel 'turn-on' fluorescent chemosensor for high selectivity and sensitivity detection of CN<sup>-</sup> based on a coumarin-Schiff base derivative in an aqueous system

Wen-Min Ding, Ya Wu, Shu-Zhen Zhang, Jing Li, Li Xu, Yin-Xia Sun

Pages: 1306-1316 | First Published: 20 April 2021



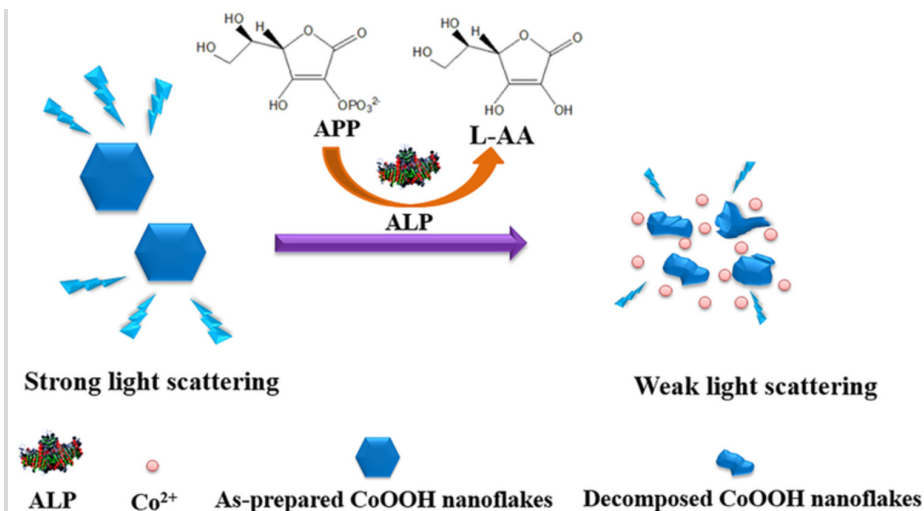
A colorimetric and fluorescent dual-channel 'turn-on' fluorescent probe **1** for CN<sup>-</sup> has been designed and synthesized. Probe **1** possessed high sensitivity and selectivity, strong anti-interference ability and wide pH range in H<sub>2</sub>O/DMSO (1:3, v/v) solution with the lowest detection limit of  $3.91 \times 10^{-8}$  M. Probe **1** was used to detect CN<sup>-</sup> in simulated water samples.

[Abstract](#) | [Full text](#) | [PDF](#) | [References](#) | [Request permissions](#)

#### Size-dependent light scattering of CoOOH nanoflakes for convenient and sensitive detection of alkaline phosphatase in human serum

Lu Ning Zhu, Ru Cheng, Kai Wen Kang, Ming Yun Chen, Tianrong Zhan, Jian Wang

Pages: 1317-1326 | First Published: 19 April 2021



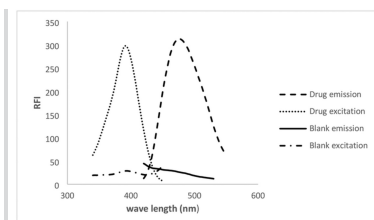
In this work, an inexpensive and simple light scattering assay was developed for the sensitive and selective detection of ALP activity in human serum, which provides new insights into develop sensitive and convenient light scattering sensors to achieve the purpose of early diagnosis of diseases.

[Abstract](#) | [Full text](#) | [PDF](#) | [References](#) | [Request permissions](#)

#### Design and strategy for spectrofluorimetric determination of tranexamic acid in its authentic form and pharmaceutical preparations: application to spiked human plasma

Ebtehal F. Anwer, Deena A. M. Nour El-Deen, Mahmoud A. Omar

Pages: 1327-1334 | First Published: 05 May 2021



Excitation and emission spectra for the reaction between tranexamic acid, ninhydrin, and phenylacetaldehyde.

[Abstract](#) | [Full text](#) | [PDF](#) | [References](#) | [Request permissions](#)

## SHORT COMMUNICATION

#### Photoluminescence studies and synthesis of BaSO<sub>3</sub>Cl<sub>2</sub>:Ce<sup>3+</sup> blue-emitting lamp phosphor

V.R. Panse, D.B. Zade, Jog Milind, S.J. Dhoble, Korhan Cengiz

Pages: 1335-1340 | First Published: 19 August 2020

[Abstract](#) | [Full text](#) | [PDF](#) | [References](#) | [Request permissions](#)

[About Wiley Online Library](#)

[Privacy Policy](#)

[Terms of Use](#)

[About Cookies](#)

[Manage Cookies](#)

[Accessibility](#)

[Wiley Research DE&I Statement and Publishing Policies](#)

[Help & Support](#)

[Contact Us](#)

[Training and Support](#)

[DMCA & Reporting Piracy](#)

[Opportunities](#)

[Subscription Agents](#)

[Advertisers & Corporate Partners](#)

[Connect with Wiley](#)

[The Wiley Network](#)

[Wiley Press Room](#)